ETR-TR-68-3

PROJECT SEE-THRU FLAME INTERFERENCE MEASUREMENTS, TITAN IIIC LAUNCH TEST 8275/2250 FINAL REPORT

Horst A. Poehler
Pan American World Airways, ASD

March 1968

New Systems Division
Directorate of Range Engineering
Air Force Eastern Test Range
Air Force Systems Command
Patrick Air Force Base, Florida

NOTICES

This report is available to agencies of the U. S. Government from Defense Documentation Center. Other requesters will secure approval of New Systems Division, Directorate of Range Engineering, Air Force Eastern Test Range, Patrick AFB, Florida, 32925.

Distribution of this document is controlled because of ethical considerations relating to tests.

When U. S. Government drawings, specifications, or other data are used for any purpose other than a definitely related Government procurement operation, the Government thereby incurs no responsibility nor any obligation whatsoever, and the fact that the Government may have formulated, furnished, or in any way supplied the said drawings, specifications, or other data, is not to be regarded by implication or otherwise, or in any manner licensing the holder or any other person or corporation, or conveying any rights or permission to manufacture, use, or sell any patented invention that may in any way be related thereto.

PROJECT SEE-THRU FLAME INTERFERENCE MEASUREMENTS, TITAN IIIC LAUNCH TEST 8275/2250 FINAL REPORT

Horst A. Poehler
Pan American World Airways, ASD

FOREWORD

This report was prepared by H. A. Poehler, Ph. D., of the Technical Staff, Pan American World Airways, Aerospace Services Division, under Contract AF 08(606)-7500 as a Final Report (internal) of Titan IIIC Test 8275/2250, to obtain data for estimating flame effects for Air Force Western Test Range flights.

The author wishes to acknowledge the contribution of the members of the RCA Telemetry and Data Translation Engineering Group, who under the direction of C. H. Goodrich, Project Engineer, were responsible for the installation of the data vans and the conduct of the flight measurements. In particular the contributions of C. H. Goodrich, Wendell Hooper, O. B. Rawls, Don Rollan, and W. L. Young deserve mention. Appreciation is also extended to Mr. R. M. Nichols of the Air Force Chemical Laboratory for the alkali-metal impurity measurements.

Variation in format is permitted in the interest of economy, legibility, and to expedite publication.

This report contains no classified information extracted from other classified documents.

This technical report has been reviewed and is approved.

FLOYD A. AMUNDSON
Lt Colonel, USAF
Chief, New Systems Division

ABSTRACT

A final report of flame attenuation, as well as flame noise measurements made at AFETR on Titan IIIC, Test 8275/2250, April 28, 1967 is presented. Measurements were made at X-band (9100 MHz), C-band (5000 MHz), S-band (2222 MHz), and P-band (220-250 MHz) frequencies at sites especially set up to yield a range of aspect angles, particularly at the low aspect angles of interest to AFWTR flights. Amplitude flame-noise measurements are reported for the first time for the Titan IIIC zero-stage. Power spectral density and probability distribution characteristics are presented. Also contained in the report are results of alkali-metal impurity measurements on the zero-stage, on the separation-rocket and the stage-I propellants; data on the effect of the exhaust flame on pulse transmission; and a plasma model of the zero-stage rocket exhaust from which predictions of rocket exhaust attenuation as a function of aspect angle and frequency can be made. The data indicates that at X- , S- , C- , and P-band frequencies, the zero-stage attenuation extends to approximately 16 degrees, measured from the roll axis. "Signal losses" at X-band reached as high as 40 db, and flame attenuation reached values greater than 23 db at S band, greater than 20 db at C band, and reached values of 20 db at P band. To alleviate the high zero-stage rocket exhaust attenuation, the imposition of a specification limiting the maximum permissible level of sodium and potassium impurity in the propellant is recommended.

TABLE OF CONTENTS

		Page No.
I.	INTRODUCTION	1
II.	PLUME NOISE DATA	2
	A. MEASUREMENT TECHNIQUES AND BANDWIDTH LIMITATIONS	2
	B. X-BAND PLUME NOISE DATA	6
	C. S-BAND PLUME NOISE DATA	16
	D. C-BAND PLUME NOISE DATA	30
	E. P-BAND PLUME NOISE DATA	33
	F. PROBABILITY DENSITY	36
III.	SPECIAL TOPICS	44
	A. EXHAUST PLUME INTERFERENCE WITH PULSE TRANSMISSION	44
	B. THRUST DECAY	49
	C. SODIUM AND POTASSIUM IMPURITY MEASUREMENTS	51
	D. EXHAUST PLUME IONIZATION MODEL	59
	E. COMPLETED OSCILLOGRAPH PLAYBACKS	69
IV.	SUMMARY OF ATTENUATION MEASUREMENTS	73
V.	ITEMS FOR NEXT TIME	75
VI.	CONCLUSIONS AND RECOMMENDATIONS	77
	REFERENCES	79
	APPENDIX	

LIST OF ILLUSTRATIONS

Figure		Page
1	AGC-Quadrature Detector Crossover Characteristic	3
2	Power Spectral Density of X-band Amplitude Fluctuations, UC-2	10
3	Power Spectral Density of X-band Amplitude Fluctuations UC-2. Composite.	13
4	Power Spectral Density of X-band Amplitude Fluctuations, UC-13	15
5	Power Spectral Density of S-band Amplitude Fluctuations, UC-13	18
6	Power Spectral Density of S-band Amplitude Fluctuations, UC-11	20
7	Power Spectral Density of S-band Amplitude Fluctuations, Composite	22
8	Power Spectrum, Amplitude Fluctuations, Zero Stage S-band, UC-11	23
9	Power Spectrum, Amplitude Fluctuations, S-band, UC-11, T + 121 Seconds	24
10	Power Spectrum, Phase Fluctuations, S-band, UC-11, T + 120 Seconds	26
11	Phase Power Spectrum, S-band UC-11, T + 60 Seconds	27
12	Power Spectral Density of S-band Phase Fluctuations, UC-11	29
13	Power Spectral Density of C-band Amplitude Fluctuations, UC-13	32
14	Power Spectral Density of P-band Amplitude Fluctuations, UC-13	35
15	Plot of Cumulative Probability of X-band Envelope Fluctuations, UC-2	38
16	Plot of Cumulative Probability of S-band Envelope Fluctuations, UC-11	39
17	Plot of Cumulative Probability of C-band Envelope Fluctuations, UC-13	40
18	Plot of Cumulative Probability of X-band Envelope Fluctuations, Separation-Rocket Exhaust, UC-2, T + 121	41

Figure		Page
19	Plot of Cumulative Probability of P-band Envelope Fluctuations, Stage-I Exhaust, UC-11	42
20	Zero-Stage and Separation-Rocket Exhaust Interference with Pulse Transmission, UC-2	46
21	Zero-Stage Exhaust Interference with Pulse Transmission, UC-13	48
22	X-band Pulse Shapes	50
23	Zero-Stage Telemetered Thrust-Decay Characteristic	52
24	Zero-Stage, Titan IIIC, SRM Plume (Vicente Model)	61
25	Titan IIIC, Exhaust Plume Ionization Model (Poehler Model)	63
26.	Electron Density Variation Along a 10^{o} Ray Through the Titan IIIC Exhaust Plume Ionization Model (Poehler Model)	
27.	Ray Through the Plume Illustrating Antenna Angles, θ, ϕ, and Aspect Angle α.	
28.	Oscillo Playback, UC-2	
29.	Oscillo Playback, UC-11	
30	Oscillo Playback, UC-13	

I. INTRODUCTION

Presented here is the final report of AFETR X- , S- , C- , and P-band measurements on Titan IIIC vehicle 10, launched on 23 April 1967, 10/01/01 GMT. The missile was instrumented with special X- and S-band transmitters. Receiver sites were set up at suitably-chosen locations, so as to yield attenuation and flame noise measurements of significance to the Air Force Western Test Range.

In an earlier report "Project See-Thru Flame Interference Measurements, Titan IIIC Launch Test 8275/2250 (Preliminary Report)," [1], the test configuration and the results of the attenuation measurements were described. The detailed test configuration and attenuation measurements are not repeated in this report. For this reason, the two reports should be considered as a unit and read together.

The engineering plan for the measurements is given in reference [2]. Departures from the engineering plan were minor. The departures are detailed in a memo by Fetner [3], and will be found reflected in the analysis given in this report.

The prime additions contained in this report are the presentation of the results of the amplitude and phase flame-noise measurements, the effect of the flame on the pulse shape, presentation of alkali-metal impurity analyses, and a rocket exhaust ionization model. In those cases where calibrations were not available for the earlier report, the missing calibrations have been supplied and the completed plots are presented. At the UC-11 and UC-13 sites, signal-strength levels were recalibrated. The corrected levels are presented.

II. PLUME NOISE DATA

The characteristics of the signal amplitude fluctuations produced by the Titan IIIC exhaust were recorded and are presented for the first time. After a discussion of the measurement techniques and bandwidth limitations, the measured statistical characteristics of the flame noise will be presented.

A. MEASUREMENT TECHNIQUES AND BANDWIDTH LIMITATIONS

1. Amplitude-Noise Characteristics

The amplitude characteristics of flame noise data were obtained by recording the output of a wide-band (10 kHz) envelope detector. The quadrature detector output was also recorded, but this provides valid envelope detection only for small phase errors ($<30^{o}$), and hence is of limited value during the major portion of the flame interference periods.

a. Low Frequency Response

The low-frequency limit for the measured amplitude flame noise characteristics is set by a) the agc bandwidth, b) the low-frequency response characteristic of the tape recorder, c) and the low-frequency pass characteristic of the bandpass filter that was used to filter the data before digitizing for statistical analysis.

The low-frequency tape recorder response extends to 300 Hz for the direct record channel of the Consolidated Electrodynamics Corporation, CEC, recorder, to 100 Hz for the Precision Instrument recorder, and to DC for the FM record channels.

Frequencies within the pass band of the agc will be removed and, therefore, will not appear at the detector output. In most cases, the pass band of the agc was less than 20 Hz. A typical agc envelope detector crossover characteristic is shown in Figure 1.

The low-frequency limit of the bandpass filter was determined by the lowest pass frequencies of the bandpass filters (Kronnhite) available for accomplishing the bandpass limiting necessary before passing the data to a digitizer. This was 20 Hz.

FIG. 1 AGC - QUADRATURE DETECTOR CROSSOVER CHARACTERISTIC
S-BAND PHASE LOCK RECEIVER, CIF SITE

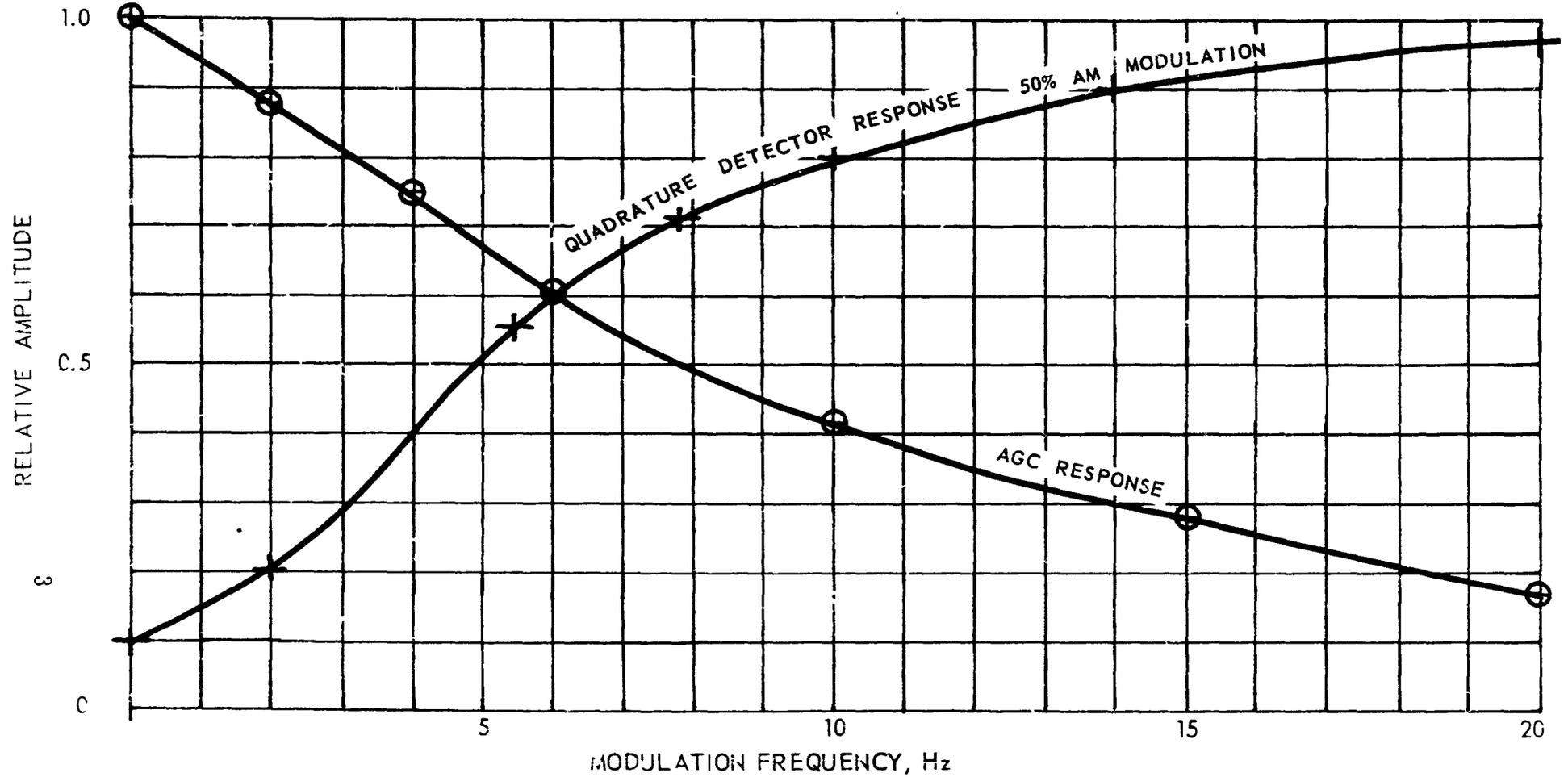

For data recorded in the FM mode, the low-frequency limit was set at 20 Hz by the agc. For data recorded in the direct-record mode, the low-pass limit was set by the tape recorder (300 Hz for CEC, and 100 Hz for the Precision Instrument Recorder).

b. High-Frequency Response

The high-frequency characteristics of the recorded data are limited by: a) the IF bandwidth; b) the high-frequency response of the envelope and phase detectors; and, c) the high-frequency response of the tape recorder.

The IF bandwidth was 3 MHz for the X-band receivers, 500 kHz for the S-band receivers, 30 kHz for the C-band receiver, and 500 kHz for the P-band receiver.

The high-frequency response of the envelope detector was 10 kHz for the envelope and for the phase detector circuits. The high-frequency response for the direct record channel was 100 kHz and for the FM record channel was 10 kHz.

The high-frequency limit in the recorded data was, therefore, set by the 10 kHz response of the amplitude and phase detectors for data recorded in the direct-record or the FM mode.

The primary high-frequency limitation in the reduced (power spectral density and probability distribution) data, however, was the 5000 sample-per-second sampling rate available at the TARE/DARE digitizer. This limited the frequency response to an ideal maximum of 2500 Hz, and a practical maximum (using 2000 Hz, 48 db/octave low-pass filters to limit aliasing) of 2000 Hz.

c. Amplitude and Noise Expressed in DB Below Carrier

The magnitude of the amplitude noise characteristics is expressed in terms of decibels below the carrier per 50 Hz bandwidth. Calibration in terms of decibels below the carrier is achieved by applying a sine wave test signal of some fixed percentage of modulation, typically 100, 50, and 25% modulation. Calibration of the phase detector was effected by unlocking the loop, producing a sinusoidal error signal of $\pm$ 90 degree (peak) phase shift at the phase-detector output. For the

calibration levels, the energy in both sidebands will be -3 db, -9 db, and -15 db below the carrier, respectively.

The receivers were equipped with agc action which, in general, held the detector output constant over a 40 db input range. Thus, the detector output will remain constant, and its percentage - modulation calibration will be valid over a 40 db range of input level variation.

In the calibrations, the input signal-strength level was varied over the range of the receiver, as a fixed percentage of modulation was applied. In those cases where the agc action did not hold the envelope detector output constant over a 40 db range, the percentage modulation calibration at the signal-strength level nearest the signal-strength level during the flame attenuation period was used in the analysis.

2. Phase-Noise Characteristics

Phase-noise characteristics were measured by recording the output of the phase detector of the phaselocked loop in the receiver.

The phase detectors used were standard and had the usual sinusoidal characteristics. For phase errors in excess of the 30 degrees, their response, therefore, is no longer linear. Parallel recording of the phase detector output using two record channels was employed. The gain of one recorder channel was set so that a 30 degree phase error would give a full-scale deflection, the other for 90 degrees, full scale.

The low-frequency limit for the measured phase noise characteristics of the flame are set by: a) the loop bandwidth of the phaselocked loop; b) the low-frequency response characteristics of the tape recorder; and, c) the low-frequency pass characteristics of the bandpass filter that is used to shape the data before digitizing.

The loop bandwidth was approximately 100 Hz for the S-band receivers, and 100 Hz for the C-band receiver.

The tape recorder and bandpass filter limitations are the same as those already discussed for the amplitude fluctuations.

For the phase-noise recordings, the actual low-frequency limit was set at approximately 100 Hz by the loop bandwidth. The high-frequency limitations are the same as those already discussed, i.e., 10 kHz for data recorded in the direct-record or FM mode.

B. X-BAND PLUME NOISE DATA

The missile carried a 1/2 microsecond, 2200 prf pulse transmitter to simulate WTR missile instrumentation. A prime object of the test was to determine the attenuation and flame noise interference for such a signal at selected sites of interest to WTR.

The attenuation data was discussed in detail in the previous report [1] and is summarized for reference in Section IV.

Quantitative flame noise data was obtained at the UC-2 and the UC-13 sites. The FCA site experienced receiver problems, and calibrations were not provided at the UC-11 site. The flame noise data obtained at the UC-2 and UC-13 sites will be discussed in this section.

1 Boxcar Demodulator

In order to determine the amplitude fluctuations that the flame imposes on the 1/2 microsecond, 2200 prf pulses sent out by the missileborne transmitter, it was necessary to construct a boxcar demodulator. In operation, a boxcar demodulator produces a pulse of the same amplitude as the incoming pulse, and holds this pulse until the next pulse comes along. It then changes its output to equal the output of the second pulse, and holds that level until the third pulse comes along, etc. The output of a boxcar demodulator, therefore, provides us with the envelope of the pulse amplitude fluctuations imposed by the flame. The pulse repetition rate, however, limits the maximum fluctuation frequency that we can detect by observing the amplitude of the pulses, as provided by the output of the boxcar demodulator. At 2200 pulses per second (2200 samples/sec) the ideal maximum frequency for which our data can yield amplitude fluctuation information is $(1/2) \cdot 2200$ or 1100 Hz.

2. Power Spectral Density and Probability Distribution

The amplitude fluctuations produced by the flame are random in nature and, therefore, need to be described in statistical terms, i.e., power spectral density and probability density. The power spectral density provides data as to the power level of the frequencies contained in the random amplitude fluctuation. The area under the probability density plot between any two amplitudes y_1 and y_2 will equal the probability that the fluctuation will have an amplitude within that range.

The limited period of flame-interference data forces us to use a sample of finite length of T seconds. Constraints on computer usage time prompt us to choose a reasonable frequency interval B, yet one that is not too small. For these reasons our power spectral density is (as is customary) an estimate $\hat{G}$ of the true power spectral density G and is given by

$$\hat{G}(f) = \frac{\overline{y_B^2}}{B}$$

where y_B^2 is the average of the squared instantaneous signal amplitude (mean square value) in a frequency interval having a bandwidth of B Hz and a center frequency of f Hz .

The uncertainty in the estimate may be defined in terms of the standard error ϵ for the sampling distribution, and is given by

$$\epsilon \approx \frac{1}{\sqrt{BT}}$$

If ϵ is less than 0.3, it may be said with 68% confidence that the true value of $G(f)$ is within the range $(1 \pm \epsilon)\hat{G}(f)$. In our case, ϵ is well below 0.3 since B = 50 Hz, T = 2 sec for most intervals, hence $\epsilon = 0.1$.

The computation of the power spectral density and the probability density was carried out on a 7094 digital computer. The analog data was digitized at 5000 samples/sec. The capability of the computer program was limited to 10,000 points, hence our time spans were limited to 2 seconds. Considering the changing nature of the data during the flight, 2-second time spans were not found to be unreasonable. In some cases, such as staging phenomena, we selected time spans of 1 and of 0.5 seconds duration.

Whereas the bandwidth of the recorded flame noise data extends to 10 kHz, the TARE/DARE digitizer available to us at AFETR has only a maximum sampling rate of 5000 points/sec. This limits the frequency of data processed by the digitizer (and therefore analyzed by the digital computer) to an ideal maximum of (1/2)·5000 or 2500 Hz, and a practical maximum (using a 2000 Hz, 48 db/octave low-pass filter to limit aliasing) of 2000 Hz. Two thousand Hertz, therefore, is the upper limit of the PSD and probability distribution data we will present in this report.

To answer the question of what flame-induced fluctuations may lie above 2000 Hz, we have employed a spectrum analyzer, with a range of 0 - 10 kHz and are, therefore, in a position to supply the answer to this question, as we shall discuss later in the report.

2. Flame-Induced Amplitude Fluctuations, Zero-Stage and Separation-Rocket Exhausts, UC-2.

The amplitude fluctuations of the 9100 MHz, 1/2 microsecond, 2200 prf pulses received at the UC-2 site were detected by a boxcar demodulator, and are shown in Figure 2 as a function of flight time.

a. Zero-Stage Exhaust

While no zero-stage attenuation was experienced at this site, flame-induced amplitude fluctuations are evident at +112 seconds, especially since they decrease with thrust (see Section IIIB) and disappear with the zero stage. The start of the flame noise period

is considered to be +70 seconds, at an aspect angle of approximately 24 degrees. The noise burst at T + 121 seconds is produced by the separation-rocket exhaust. The extent of the separation-rocket exhaust flame was discussed and illustrated in the companion report [1] to which the reader is referred for details. The noise prior to T + 60 is front-end noise, resulting from the poor signal/noise ratio (excepting for a burst around T 0 which likely is attributable to the exhaust flame which surrounds the missile at ignition).

Power spectral density plots are shown in Figure 2, each plot referenced to a corresponding flame-noise period on the envelope detector record. The shaded bar on the PSD plots has been added to afford a basis of comparison in the levels shown in the flame (80-82, 90-92, 99-101, 103-105, 110-112, 121-122) and non-flame (62-64, 117.5-119.5) plots. It has no further significance.

It is apparent from these plots that the energy of the signal fluctuations (changes in pulse height) produced by the rocket exhaust has the greatest value at the low frequencies. As the frequency increases, the energy of the flame-induced signal fluctuation decreases. This decrease agrees with the data obtained in static firings reported by Williams [4] and Smoot [5], as well as with theoretical predictions from turbulent scattering models by Geiger [6] and Williams [4]. Since the pulse sampling rate was limited to the prf of 2200 per second, no flame noise data should be read into (or can be obtained) from these plots at frequencies higher than (1/2)·2200 or 1100 Hz. The power shown on the PSD plots above 1100 Hz represents the background noise level.

The quantitative data provided by these plots is significant, since it indicates the flame noise power in the sidebands to be as high as 18 db below the carrier per 50 Hz bandwidth. Note that the higher value of 16 db below the carrier shown in Figure 2 cannot be taken as the maximum value of the flame noise power because of the high level of background noise (no-flame PSD) at this instrumentation site. The power spectral density of the background noise must always be subtracted from the flame-noise power spectral density. Note, however, that the PSD plots shown in Figure 2, and in subsequent plots, are in decibels. The

FIG. 2 POWER SPECTRAL DENSITY OF X-BAND AMPLITUDE FLUCTUATIONS DURING FLIGHT, ILLUSTRATING THE SEVERE MODULATION PRODUCED BY THE ZERO-STAGE AND SEPARATION ROCKET EXHAUSTS. UC-2, TEST 8275/2250, APRIL 28, 1967, 9100 MHz, 1/2 MICROSECOND, 2200 PRF PULSES. PSD OF THE OUTPUT OF A BOXCAR DEMODULATOR.

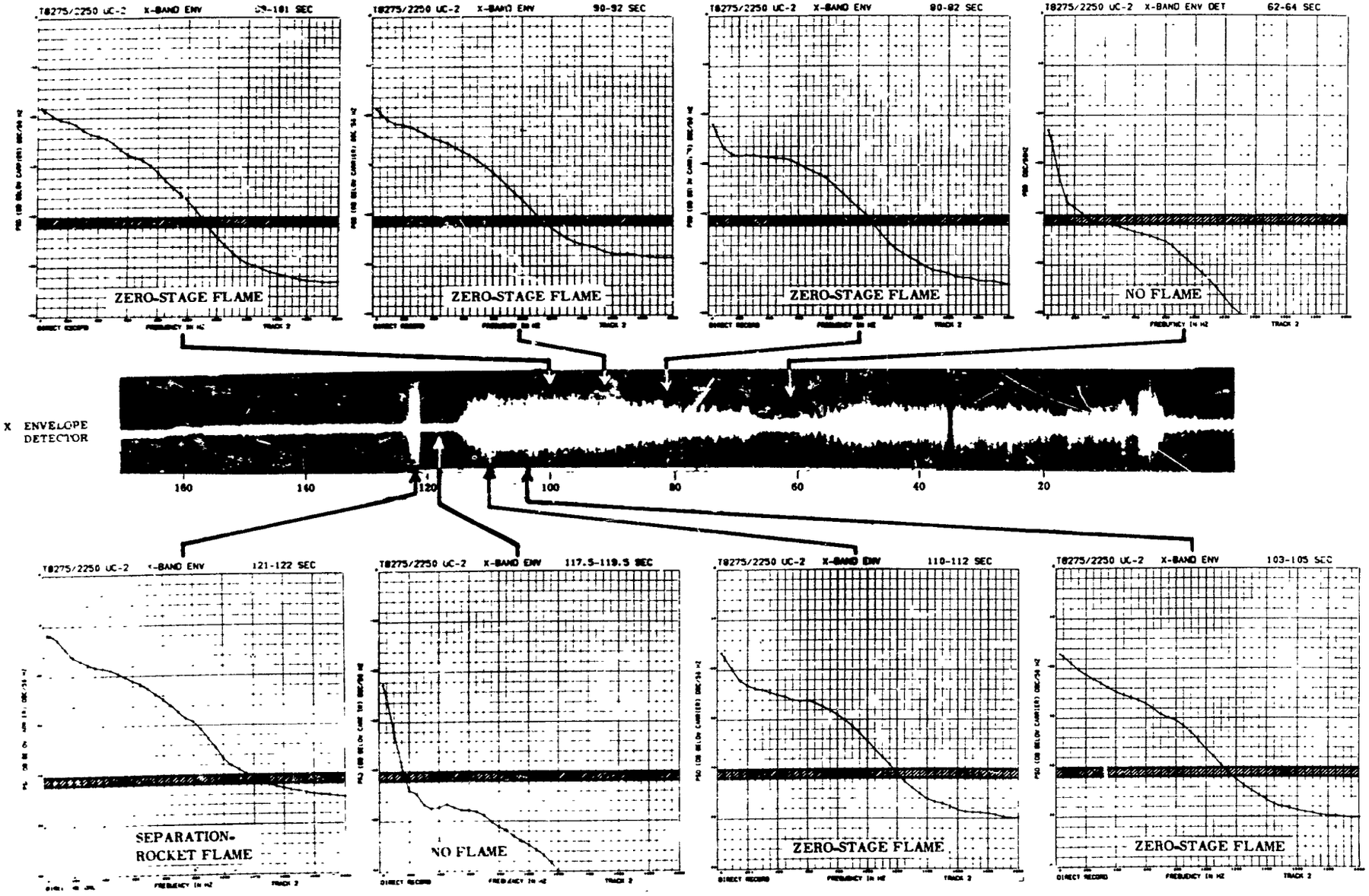

necessary subtraction cannot be made when expressed in decibels, hence cannot be made by taking the difference in the heights of the PSD curves shown in Figure 2. The decibel values must first be converted to units of power. The background noise level may then be subtracted. The remainder is the flame noise power, which may then be converted to decibels and expressed in decibels below the carrier.

It is also significant that flame noise can be severe even when there is no attenuation. Our measurements do not indicate attenuation* during the 70 - 115 second period during which the flame noise shown in Figure 2 is evident. Similar observations have frequently been made at AFETR in the past on various missiles [7], [8] . The aspect angles over which flame noise manifests itself is always greater than the aspect angles over which attenuation can be noted.

It is evident from the data shown in Figure 2 (and from the aspect angle data of Figure 28) that plume noise extends to as far as 24 degrees from the missile roll axis. For reference, the attenuating portion of the plume extends to 16 degrees (see Section IV).

b. Separation-Rocket Exhaust

Zero-stage separation is accomplished by the operation of sixteen staging rockets whose axis is transverse to the missile roll axis, and whose exhaust envelops the Titan IIIC missile in flame. Photographs of the staging event, as well as a detailed description of the location and operation of the separation rockets, have already been given in an earlier report [9] .

The separation-rocket exhaust is highly attenuating, and the exhaust interference extends to aspect angles considerably beyond the 16 degrees of the attenuating zero-stage exhaust.

---

* Note, however, that since the uncertainty of our measurement is of the order of 3 db, 1 - 2 db attenuation could be present.

The noise produced by the separation-rocket exhaust is clearly visible as a severe noise burst at 121 seconds. The noise amplitude during separation-rocket operation exceeds the noise amplitude during the zero-stage operation. As the PSD plot in Figure 2 shows, the power spectral density of the amplitude fluctuations produced by the separation rocket exhaust is higher than that for the zero-stage exhaust, and reaches a value as high as 12 db below the carrier over the 50 Hz bandwidth centered at 25 Hz.

Reference to Figure 28 shows that the separation rockets produce an attenuation of some 10 db at the UC2 site (aspect angle 15 degrees) and therefore an attenuation of 10 db is to be associated with the flame noise shown at +121 seconds.

A composite PSD plot which illustrates the increase in the power spectral density produced by the zero-stage exhaust, and the further increase produced by the separation rocket exhaust is shown in Figure 3.

The quiescent noise level for the no-flame period (117.5 - 119.5 seconds) is some -45 db below the carrier per 50 Hz bandwidth. The zero-stage exhaust flame causes an increase of some 20 db in the measured amplitude noise. The power spectral density separation-rocket exhaust noise exceeds that of the zero-stage exhaust noise by some 5 db.

4. Flame-Induced Amplitude Fluctuations, Zero-Stage and Separation Rocket Exhausts, UC-13

Data collected at the UC-13 site provides us with flame-induced amplitude fluctuations of the 9100 MHz, 1/2 microsecond 2200 prf pulses for transmission paths that penetrate the flame more deeply than at UC-2. Aspect angles, signal-strength, and boxcar detector output recorded at UC-13 are shown in Figure 30 page 72.

As already discussed in the companion report [1], signal strength drops abruptly at T+56 seconds, at an aspect angle of 35 degrees.

FIG. 3 POWER SPECTRAL DENSITY OF X-BAND AMPLITUDE FLUCTUATIONS, DURING FLIGHT. COMPOSITE UC-2 TEST 8275/2250, APRIL 28, 1967, 9100 MHz, 1/2 MICROSECOND, 2200 PRF PULSES PSD OF THE OUTPUT OF A BOXCAR DEMODULATOR

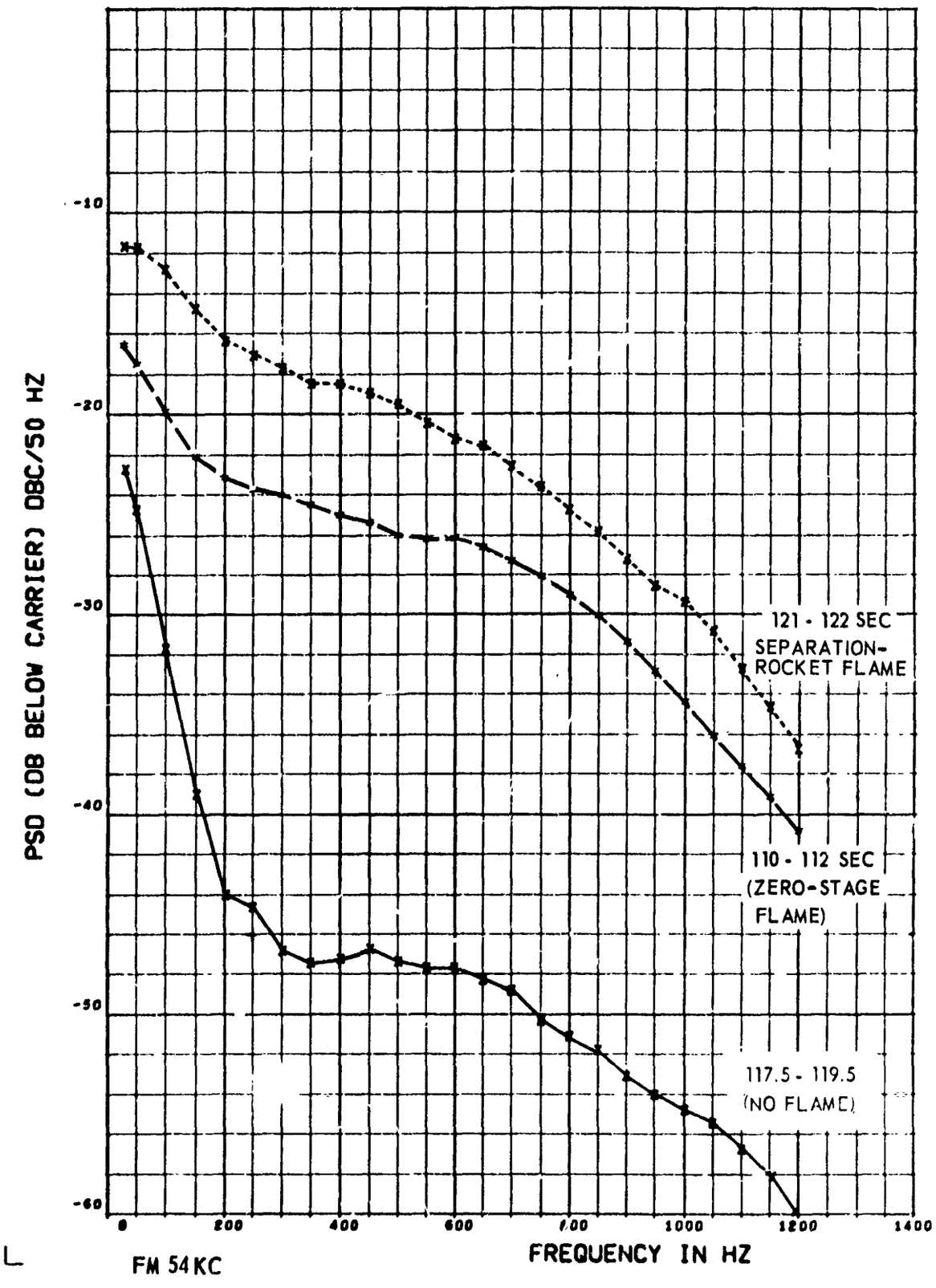

Track is lost for reasons that are not resolved, but definitely not considered ascribable to flame, because of the wide aspect angle and the character of the noise.

Track is recovered at + 95 seconds. Attenuation is apparent until + 110 seconds. Cessation of attenuation at + 110 seconds coincides with thrust decay of the zero stage (see Figure 23, page 52. Cessation of attenuation with thrust decay is reliable evidence that the attenuation was really caused by flame attenuation and not by cross polarization, antenna pattern, or loss of track. Cessation of attenuation with thrust decay has been observed on other missiles. For a more detailed discussion, see reference [7] .

As can also be seen from Figure 30, flame noise extends beyond the cessation of attenuation (at + 110) . Fast-speed playbacks show it to continue through thrust tailoff till + 113. 5 seconds.

At UC-13, we are left with only 19 seconds of flame noise data, + 95 - 114 seconds. The loss of track at + 56 seconds was most unfortunate. However, the loss of track is not the only reason for the brief noise data span. The site was located too deep in the flame region. Large attenuation combined with a modest signal margin would have served to put the signal near threshold from + 70 to + 95 even if the antenna had been on track.

It should be observed that if the object is to obtain flame noise data, we should not locate the site so deep in the flame as to bring the signal near threshold. Any noise data collected in this way will be of very limited value, since it will be corrupted by receiver front-end noise.

The results of the power spectral density of selected segments of the zero stage (95 - 114 seconds) and separation rocket (121 - 122 seconds) flame-noise data are presented in Figure 4, together with a record of the envelope detector (boxcar) output. Each PSD plot is referenced to the appropriate portion of the envelope detector record.

The data is very similar to that already presented and discussed for UC-2 in spite of some one-sided clipping evident in the UC-13 record. The separation-rocket exhaust again produces a more

FIG. 4 POWER SPECTRAL DENSITY OF X-BAND AMPLITUDE FLUCTUATIONS DURING FLIGHT, ILLUSTRATING THE SEVERE MODULATION PRODUCED BY THE ZERO-STAGE AND SEPARATION ROCKET EXHAUSTS. UC-13, TEST 8275/2250, APRIL 28, 1967, 9100 MHz, 1/2 MICROSECOND, 2200 PRF PULSES.

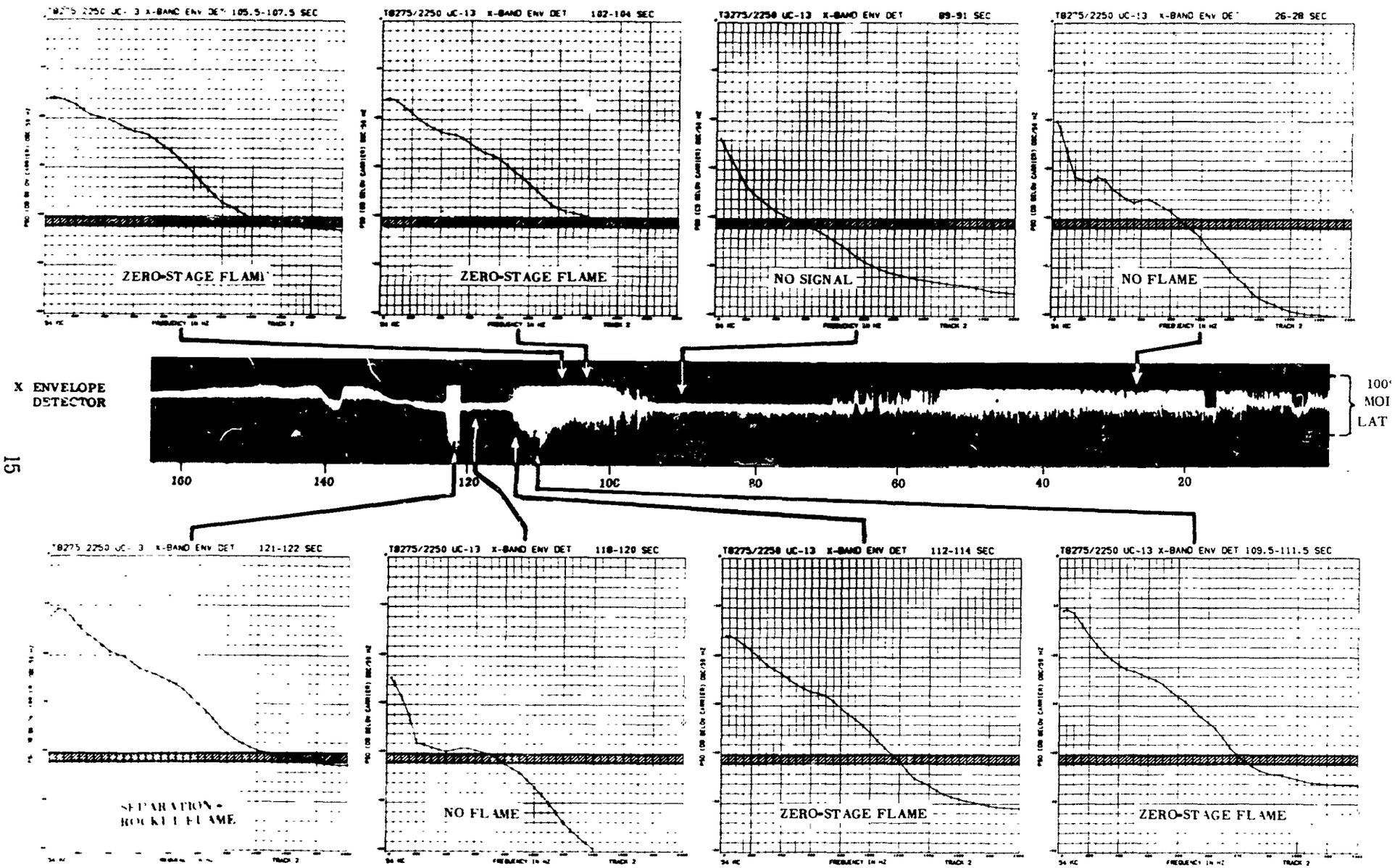

severe noise modulation than does the zero-stage exhaust.

A surprising result is that the amplitude of the flame noise at UC-13 is not appreciably higher than that at UC-2, in spite of the fact that the transmission path to UC-13 penetrates deeply into the flame and the transmission path to UC-2 lies outside the attenuation portion of the flame. It should be pointed out, however, that our data on this point is limited and therefore a firm conclusion on this point should be reserved until verified by more substantial data

Additional power-spectral-density analyses were conducted early in flight (26 - 28, multipath and noise), for no signal (89 - 91), and for no flame (116 - 120) periods. The power below 100 Hz reflects instrumentation problems (hum, pickup) and should be ignored.

Some one-sided clipping, evident in the record, resulted from improper level setting of the recorders during test. The other X envelope detector record shown in Figure 30 was recorded in the direct-record mode and is not clipped. However, it could not be used for a quantitative PSD because its calibration was not provided.

C. S-BAND PLUME NOISE DATA

1. Instrumentation and Setup

Instrumentation was set up to obtain S-band attenuation and flame noise data at the UC-2, UC-11, UC-13, CIF and FCA Building sites. Antenna acquisition and hum problems were encountered at the FCA Building site rendered FCA data of little value. The attenuation measurements were discussed in detail in the companion report [1] . For convenience, a summary of the attenuation measurements is given in Section IV.

Useful plume noise data was obtained at the UC-11 and UC-13 sites. As Figure 28 shows, the recording of the S-band envelope detector data at the UC-2 site is overloaded with an intermittent random noise of such intensity as to render the data useless.

The CIF site, while just outside the flame attenuation zone, exhibited evidence of flame noise (see Figure 15 of the companion report [1]

similar to UC-2 X-band experience (see Section IIB), where flame noise was noted t aspect angles beyond the attenuation zone. Also, evident in the C' ' record are continuing unlocks of the phase lock receiver because of the severe phase unstability of the S-band missile-borne transmitter (see Figures 10 and 11, and associated discussion given later in this report). Because of the continuing unlocks, no useful S-band data was obtained at the CIF sites.

At UC-11 and UC-13 Defense Electronic Industries TMR-5A telemetry receivers with THM-M5B tuning units were used to receive the S-band signal. These receivers did not have long- or short-loop tracking capability, hence it was not possible to use the planned 30 kHz IF bandwidth; instead a 500 kHz IF bandwidth was used, together with an envelope detector. A shortage of the TMR-15 receivers, equipped with long-loop tracking capability, dictated the use of the TMR-5A receivers at UC-11 and UC-13.

2. Amplitude Noise Data

a. UC-13 Site

Useful amplitude noise data was obtained at UC-13 during zero-stage and separation-rocket operation. This data is presented in Figure 5 in which power spectral density plots of flame induced amplitude fluctuations of the S-band 2222MHz signal received at UC-13 are shown as a function of flight time.

Also shown is the envelope detector record. Each PSD plot is referenced to the segment of the envelope detector record to which it corresponds.

For an identification of the flame-noise portion of the envelope detector record, reference to Figure 30 is necessary. Flame attenuation at this site was so severe that the signal was lost at the onset of flame attenuation (T + 74) and was not regained until the thrust-decay period had started (T + 110). Hence only a few seconds of zero-stage flame noise during the short decay period (110 - 114 seconds) are available. A PSD plot (110.5 - 112.5) of the amplitude flame noise during this period shows an amplitude flame noise characteristic similar to that already shown for X-band, except that the noise

FIG. 5 POWER SPECTRAL DENSITY OF S - BAND AMPLITUDE FLUCTUATIONS DURING FLIGHT, ILLUSTRATING SEVERE MODULATION PRODUCED BY THE ZERO - STAGE AND SEPARATION ROCKET EXHAUST UC - 13 2200 MHz PSD OF ENVELOPE DETECTOR OUTPUT

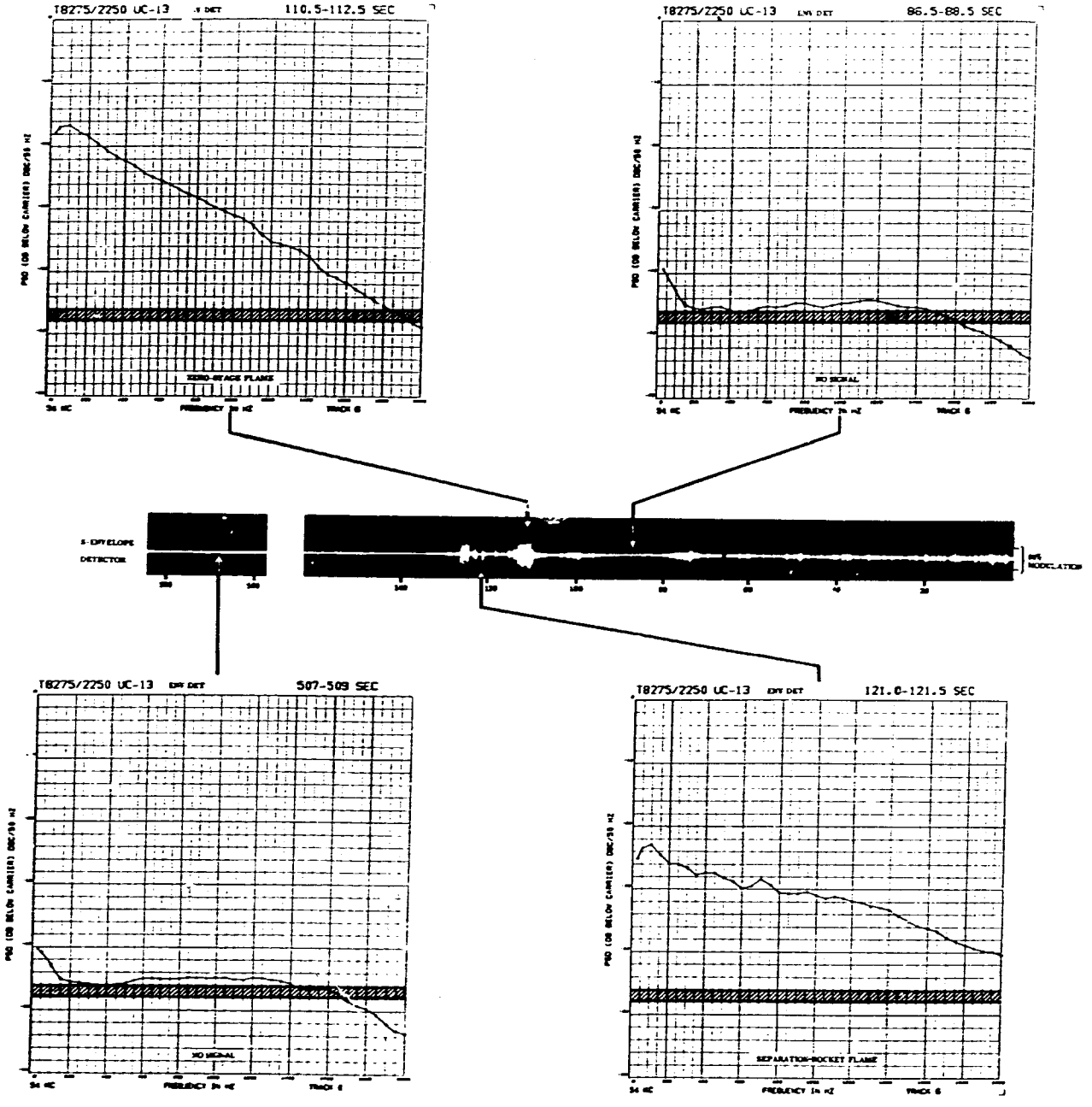

now extends to 2000 Hz (the limit of our PSD analysis capability). PSD levels of the S-band flame noise of as high as - 17 db below the carrier per 50 Hz bandwidth are indicated at 100 Hz. The FM record mode used extended the data to as low as 20 Hz (see Section II A) .

Separation rocket amplitude modulation is visible at 121 seconds, and a PSD plot (121.0 - 121.5) shows the noise to be high, but less intense than during zero-stage.

As a control, PSD plots were also run for the 86.5 - 88.5 and the 507 - 509 second spans. During these periods the receiver is at its threshold, and therefore the PSD plot should be that of white noise. The small decay above 1600 cycles is due to the 2000 Hz, 48 db/ octave band-limiting filter that was required to band limit the data before digitizing. Since there is no carrier signal during these time intervals, the ordinate "db below carrier" has no significance in these plots. The noise is essentially white, as it should be.

b. UC-11 Site

The amplitude flame noise data collected at UC-11 is shown in Figure 6. Power spectral density plots of the amplitude noise are shown together with the envelope detector record and referenced to the time segments of the record to which they refer.

As discussed in the companion report [1], the drop in signal (see Figure 29) that occurs at + 75 seconds (16 degree aspect angle) is attributed to flame attenuation. The operator's efforts to modify antenna pointing raises doubts about the track until + 90 seconds. Primarily because UC- 11 was located so deep in the flame (very low aspect angles), only a few seconds of flame attenuation data near the end of zero stage and during thrust decay was obtained. A PSD analysis of a segment of this data during zero stage (108 - 110) and during thrust decay (112 - 114) was run. Also shown is a plot of the power spectral density during separation rocket firing (122.2 - 122.7). The signal amplitude fluctuations produced by the flame include frequencies up to 2000 Hz (the limit of our analysis). Two intervals were run as controls. The zero-stage rocket thrust has decayed to zero at 117 - 119, and only

FIG. 6 POWER SPECTRAL DENSITY OF S-BAND AMPLITUDE FLUCTUATIONS DURING FLIGHT, ILLUSTRATING THE SEVERE MODULATION PRODUCED BY THE ZERO-STAGE AND SEPARATION ROCKET EXHAUSTS. UC-11, TEST 8275/2250, APRIL 28, 1967, 2200 MHz, PSD OF ENVELOPE DETECTOR OUTPUT

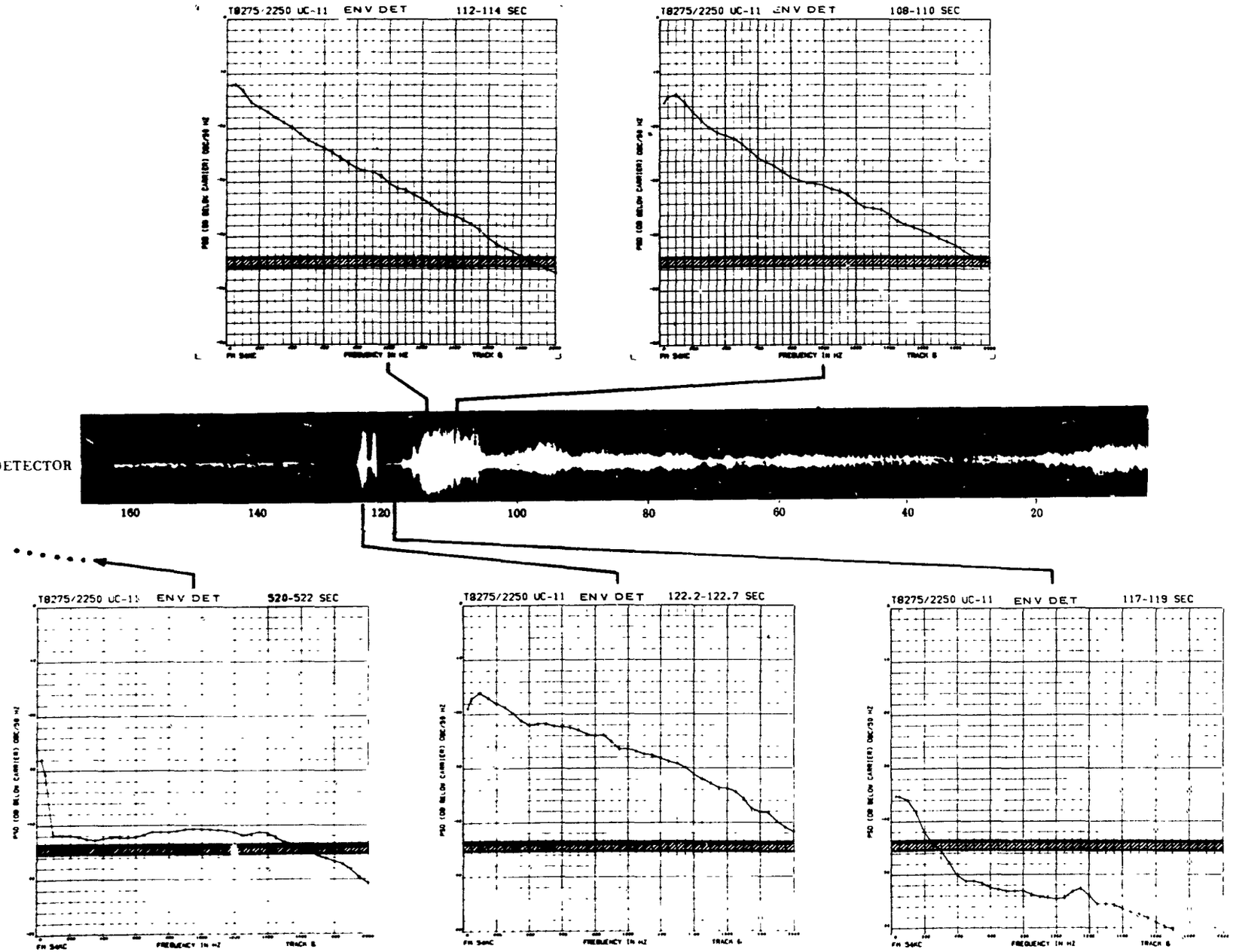

the liquid stage exhaust remains. Clearly the liquid-propellant exhaust flame does not modulate the S-band signal. Noise power levels of as low as -50 db below the carrier are noted. The noise below 200 Hz is not attributable to the flame but to instrumentation noise. The plot at 520 - 522 seconds is presented to illustrate noise threshold. Since there is no carrier signal at this time, the ordinate "db below carrier" has no significance for this plot. The noise is essentially white, as it should be. Instrumentation noise is noted below 100 Hz, and the dropoff at 1600 Hz is attributed to the 2000 Hz, 48 db/octave, low-pass filter used to bandlimit the data before digitizing.

A composite plot of UC-11 S-band amplitude PSD data illustrates the increase in power spectral density produced by the zero-stage exhaust, and the further increase produced by the separation-rocket exhaust is shown in Figure 7.

3. Amplitude Power Spectrum Above 2 kHz

As has already been pointed out, all the PSD plots presented in this report are limited to 2 kHz at the high end. This limitation arises not from the recorded data (which extends to 10 kHz) but from the maximum sampling rate of 5000 points/sec of the TARE/DARE digitizer available to us at AFETR.

In order to provide an answer to the question of what flame-induced fluctuations may lie above 2 kHz, we have employed a spectrum analyzer with range 0 - 10 kHz, and have photographed the displayed spectrum output. The power spectrum of the envelope detector output waveform was observed and photographed as a function of the flight time.

Typical of the results observed are the power spectrum photographs shown in Figures 8 and 9.

The spectrum in Figure 8 indicates that amplitude noise power of the zero stage does extend beyond 4 kHz. The low signal-to-noise ratio, however, has raised the resistor noise level (white noise) making it difficult to isolate the flame noise - especially above 4 kHz. In order to obtain this data on the next test it will be necessary to select

FIG. 7 POWER SPECTRAL DENSITY OF S-BAND AMPLITUDE FLUCTUATIONS DURING FLIGHT. COMPOSITE UC-11, TEST 8275/2250, APRIL 28, 1967, 2222 MHz. PSD OF THE ENVELOPE DETECTOR OUTPUT.

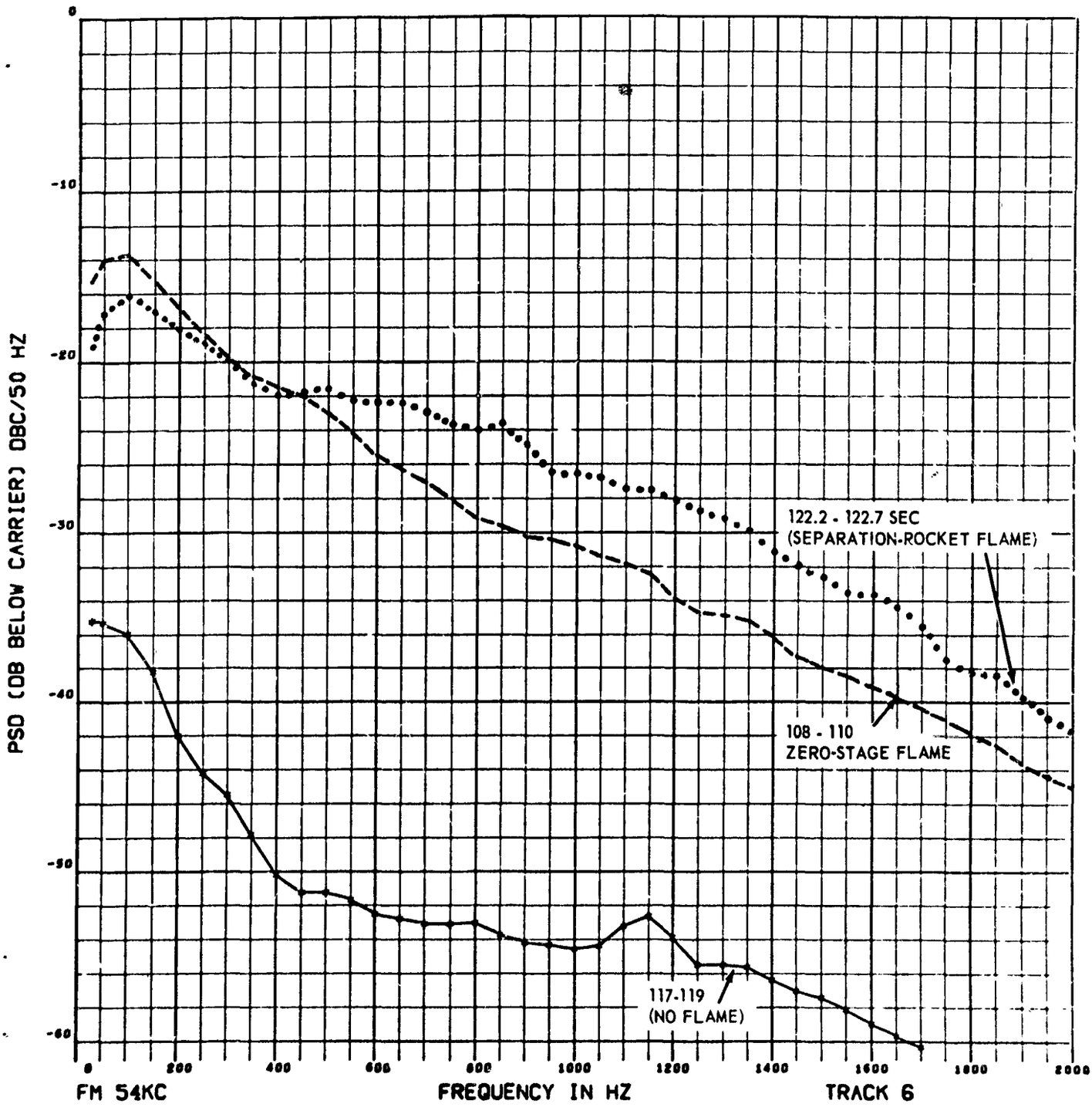

FIG. 8 POWER SPECTRUM, AMPLITUDE FLUCTUATIONS PRODUCED BY ZERO-STAGE FLAME INTERFERENCE. T+ 110 SEC. UC-11, S-BAND (2222 MHz) OUTPUT OF ENVELOPE DETECTOR.

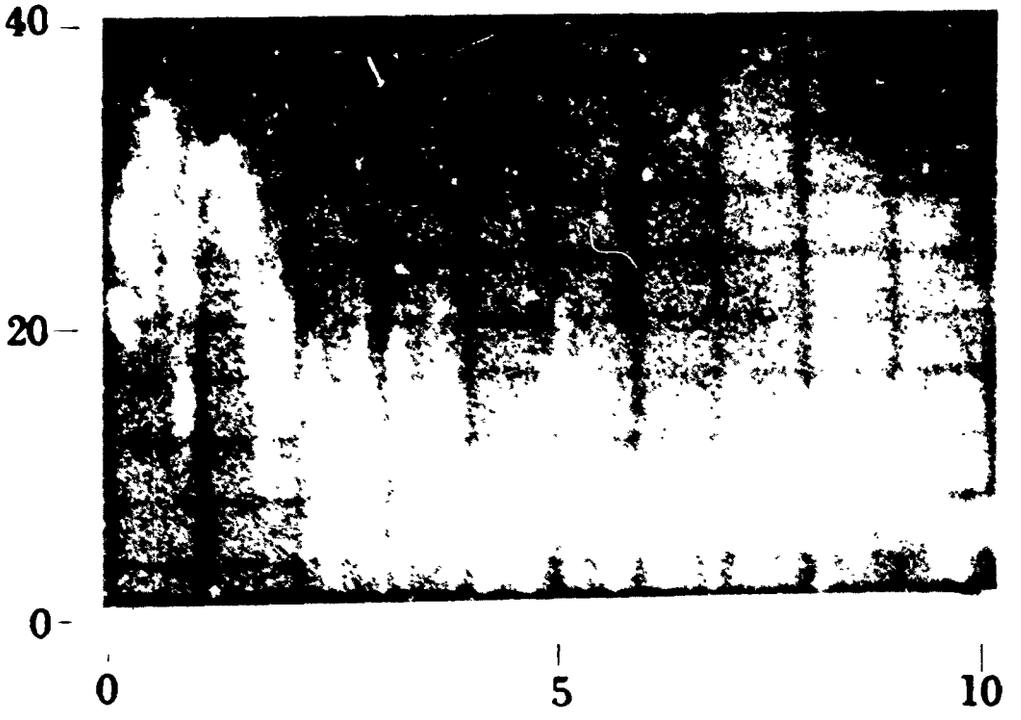

FIG. 9 POWER SPECTRUM, AMPLITUDE FLUCTUATIONS DURING ZERO-STAGE SEPARATION. OUTPUT OF ENVELOPE DETECTOR UC-11, S-BAND (2222 MHz), T + 121 SEC.

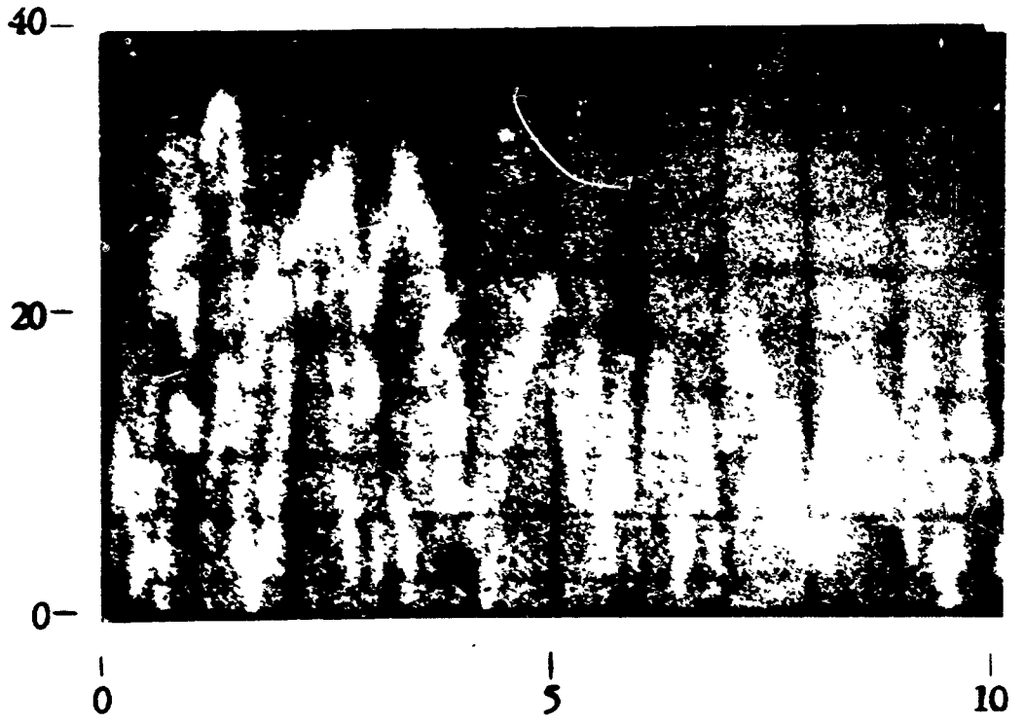

a site so positioned as to experience flame attenuation, but also so positioned that the signal/noise ratio during the flame period is not too low. Further, we recommend dual recording of the low and high-frequency portions of the flame noise spectrum to prevent overloading by the higher-energy, low-frequency components.

The power spectrum of the separation-rocket exhaust modulation shown in Figure 9 shows amplitude flame noise components up to 10 kHz and illustrates the increased noise level of the separation-rocket exhaust flame.

4. Phase-Noise Data

a. Instrumentation, and Frequency Stability Problems

Instrumentation was set up to obtain S-band phase noise data at the UC-2, UC-11, UC-13, CIF, and FCA Building sites. Unfortunately, phase noise data was not obtained at any site.

Antenna tracking problems eliminated data from the FCA Building site. Failure to obtain phase data at UC-2, UC-11, UC-13, and CIF sites is primarily due to the excessively high level of phase modulation in the supposedly clean CW missleborne S-band transmitter. Phase lock tracking requires a highly stable transmitter. The S-band missile-borne transmitter was by no means of the necessary frequency stability.

The CIF site was outside the flame attenuation zone, yet the phaselock receiver continually unlocked, even at high S/N ratios.

At UC-13, the phase detector output showed such a high level of noise output even during the non-flame period, that the phase data at this site could not be considered valid.

The unwanted phase modulation on the S-band signal is illustrated in the power spectrum of the phase detector output at UC-11 during a non-flame period (T + 120) shown in Figure 10. Note the modulation at 1.8 and 7 kHz. A further illustration is given in Figure 11. Here the spectrum of the phase detector output during a non-flame period (T + 60 seconds) is shown. This time, however, the signal strength is

FIG. 10 POWER SPECTRUM, PHASE FLUCTUATIONS ILLUSTRATING UNWANTED MODULATION PRESENT ON S-BAND TRANSMITTER. OUTPUT OF PHASE DETECTOR.
UC-11, T+ 120 SEC. (NON-FLAME PERIOD)

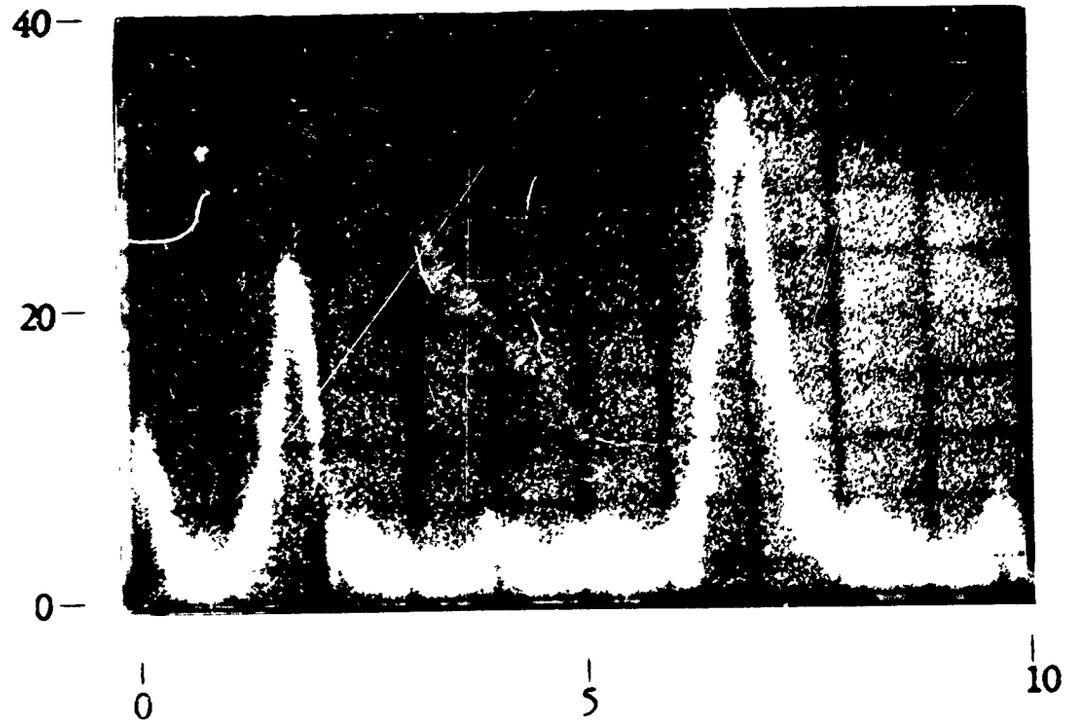

FIG. 11 PHASE POWER SPECTRUM. ILLUSTRATING THE UNWANTED MODULATION PRESENT ON S-BAND TRANSMITTER. OUTPUT OF PHASE DETECTOR UC-11, T+60 SEC. (NON-FLAME PERIOD)

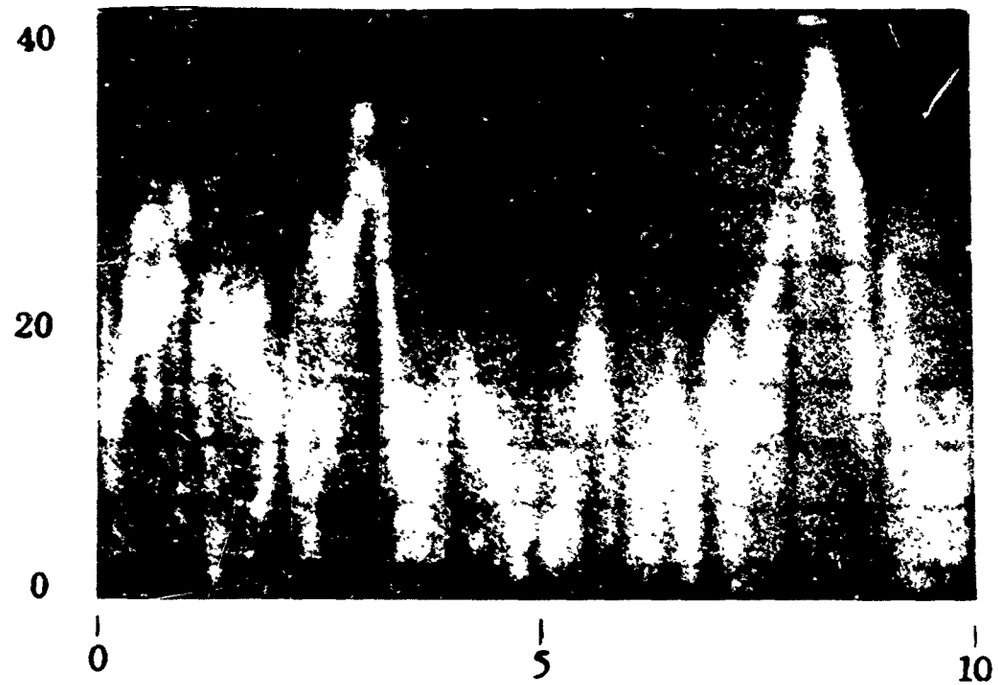

some 15 db lower and receiver front-end noise is evident at a signal strength of -100 dbm. Note that the modulation of the S-band signal is unstable and now shows up at 3 and 8.3 kHz. The phase noise of the transmitter is some 20 db above the front-end noise level. Clearly the S-band missileborne transmitter is unsatisfactory.

It is interesting to note that we were able to use the phase noise on the S-band signal for a useful purpose. No recording of phaselock indication had been provided in the test data, and we are at first hard put to determine from the data as to when the receiver was phaselocked. The undesired modulation in the S-band signal provided us with the desired phaselock indication. When the 8 kHz noise peak appears in the spectrum of the phase detector output, clearly the receiver is phaselocked. This provides the answer we are seeking.

b. Phase Noise Data, UC-11

No phase noise data was obtained even at UC-11, because the phase lock receiver became unlocked during the flame interference periods, 74 - 114 and 121 - 122 seconds. The failure to maintain phase lock was due to the excessive level of unwanted phase modulation of the S-band transmitter.

As pointed out in Section II-C-4a, the phase modulation peaks of the S-band transmitter can be used as an indicator of lock/unlock. When the transmitter phase peaks at 1.6 kHz and 7 kHz appear in the spectrum or in the PSD of the phase detector output signal, the receiver is locked. When these peaks do not appear, the receiver is unlocked. With this in mind, the reader is referred to Figure 12, which shows composite power spectral density plots of the phase detector output signal fluctuations at 110 - 111.5 (zero stage flame), at 117 - 119 (no flame), and at 121 - 122 seconds (separation-rocket flame).

During the no-flame period (117 - 119) the receiver is locked, as the peak at 1600 Hz demonstrates. "No flame", strictly speaking, means no zero-stage solid propellant flame. There is, of course, the liquid-propellant flame of stage I. The stage-I flame, however,

FIG. 12 POWER SPECTRAL DENSITY OF S-BAND PHASE FLUCTUATIONS DURING FLIGHT UC-11, TEST 8275/2250, APRIL 28, 1967, 2222 MHz. PSD OF THE PHASE DETECTOR OUTPUT

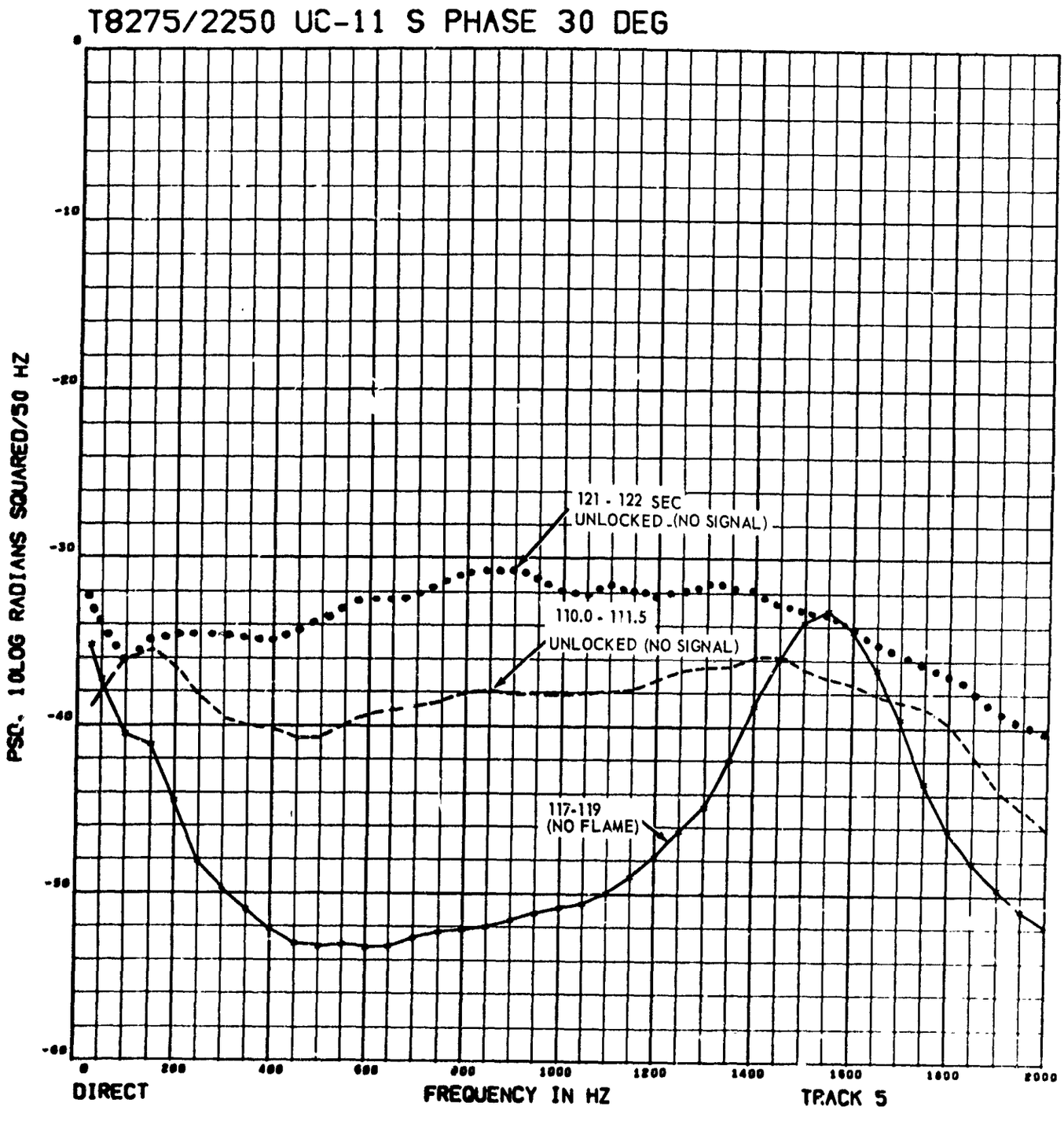

does not attenuate or introduce flame noise on S-band signals. As we shall see later, however, this is not true at P-band (250 MHz).

During the zero stage (110 - 111.5) and separation-rocket (121 - 122) flame periods, the receiver is clearly unlocked as evidenced by the absence of the S-band transmitter peak at 1600 Hz, and as evidenced by the flat, white noise PSD characteristic.

If the phase noise characteristics of the flame are to be obtained on the next test, it is essential that the S-band transmitter be redesigned to remove the intolerable amount of phase noise present on its signal.

D. C-BAND PLUME NOISE DATA

Instrumentation was set up to obtain C-band attenuation and flame noise data at the FCA Building and at the UC-13 sites. Receiver and antenna problems were experienced at the FCA site. The high noise level and hum in the data collected at the FCA site make this data of little value.

Attenuation and flame noise data were obtained from the C-band Glotrac van that was stationed at UC-13. The attenuation measurements were discussed in detail in the companion report [1] . A summary of the results is given in Section IV.

The data showed that the position of the UC-13 site was not favorable to obtaining flame noise data because its location deep in the flame (aspect angle < 6 degrees from 85 to 110 seconds, with a minimum of 2 degrees at 90 seconds) added to an extremely unfavorable antenna pattern to this site because the antenna was on the other side of the missile during a major portion of zero-stage operation.

As the signal-strength data of Figure 21 of the referenced report [1] shows, signal was lost from +74 to 110 seconds. This loss is due to flame attenuation. In short, during the major portion (some 36 seconds) of the flame attenuation period, we have no flame noise data. The receiver was at its threshold. An obvious lesson to be remembered

next time -- in order to obtain flame noise data, locate the receiver so that the signal will be attenuated, but do not locate the receiver so that the combined operation of an unfavorable antenna pattern and flame attenuation will cause the received signal to fall below threshold during the major portion of the flame-attenuation period.

The failure to obtain C-band flame noise data over the major portion of the flame interference period is particularly unfortunate because of the phase instabilities of the S-band transmitter, already discussed. The C-band transponder not only does not exhibit the severe phase instability of the S-band transmitter, but moreover is coherent. Valuable amplitude and phase noise could have been obtained from the Glotrac system had the location been more favorable. Because of the phaselocked operation and inherent stability of the Glotrac system, it is strongly recommended that a measurement be made with a Glotrac van suitably located on the next two or three Titan IIIC tests, so that the much-needed phase noise data can be obtained.

In spite of the problems just discussed, a few seconds of flame noise data were obtained -- during the thrust-decay period (+ 110 - 114 seconds) and during the separation-rocket firing period (121 - 122). The amplitude fluctuations produced by the zero-stage and separation-rocket exhaust flames are evident on the envelope detector and quadrature detector records, as well as on the power spectral density plots shown in Figure 13. For reference, signal strength is also shown.

The highest flame noise level shown is that around + 112 seconds, for which a power spectral density plot is shown. Flame modulation frequencies are seen to extend to 2000 Hz (the limit of our analysis capability), and the power level reaches - 20 db below the carrier per 50 Hz bandwidth at low frequencies. This power level is less than that found for X- and S-band during zero stage. However, it must be kept in mind that the - 20 dbc shown in the 110 - 112 second plot occurs during the thrust-decay period (see Figure 23), and therefore we should expect the flame noise to be less severe.

FIG. 13 POWER SPECTRAL DENSITY OF C - BAND AMPLITUDE FLUCTUATIONS DURING FLIGHT
UC - 13 5000 MHz PSD OF THE ENVELOPE DETECTOR OUTPUT

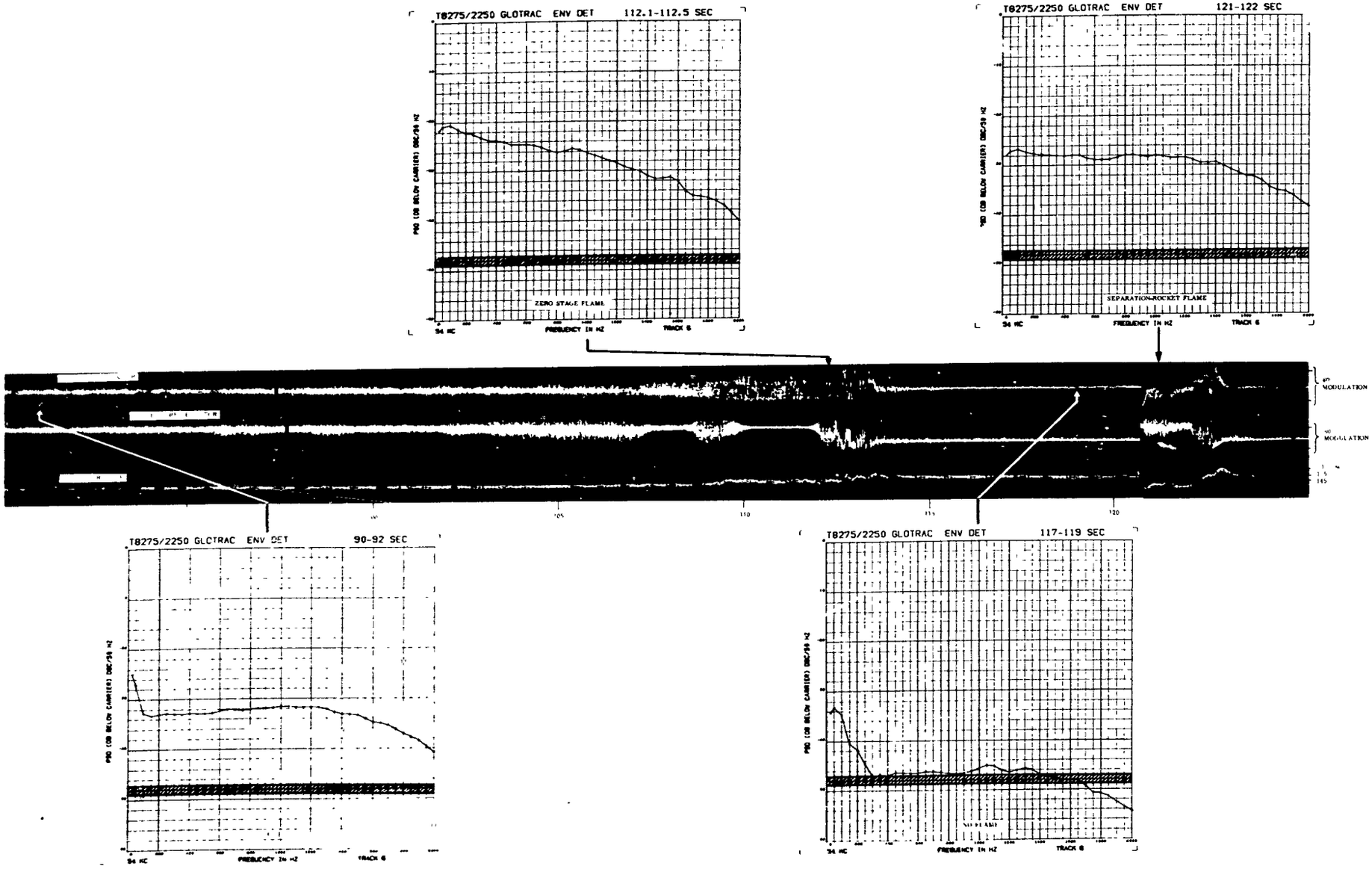

In the period 115 - 121 seconds, the zero-stage thrust has decayed to zero and only the Stage-I flame exists. Note the corresponding decrease in the flame noise on the envelope detector and quadrature detector records and in the 117 - 119 second PSD plot.

Flame noise increases during the zero-stage separation rocket operation (121 - 122), but not to the high level noted during the zero-stage thrust decay period (110 - 112) .

The envelope detector noise output when the receiver is at threshold is indicated by the 90 - 92 second PSD plot. Since there is no carrier signal at this time, reference to db below the carrier has no significance for this plot.

E. P-BAND PLUME NOISE DATA

P-band attenuation and amplitude noise data were collected at UC-11 and UC-13. The attenuation data were presented in the companion report [1], and are summarized in Section IV.

The missile carried three PCM/FM telemetry links. Flame-induced amplitude fluctuations on the 240. 2 and 249. 9 MHz PCM/FM links. Fortunately, the residual AM modulation on these links was sufficiently below the flame-induced modulation to make this measurement possible.

Useful amplitude noise data was obtained during stage-I operation on the 249. 9 MHz link at the UC-11 and the UC-13 site. Operational problems were encountered in the 240. 2 MHz measurement. The high noise levels on this data makes is unusable.

The amplitude noise data collected during zero stage appears questionable and, therefore, is not presented. The envelope detector output appears erratic, and, in particular, zero-stage thrust decay phenomena was not evidenced. Fetner's memo [3] makes specific reference to "catastrophic failure experienced by the P-band envelope detector at UC-13" occuring shortly before launch. "Data is degraded, but is believed to be usable."

Power spectral density analyses during zero-stage and separation-rocket operation were, for the most part, 35 decibels below carrier level, and had the general appearance of white noise. Unfortunately, therefore, no zero-stage noise data is available.

Some useful data was obtained during stage-I operation and at stage II-ignition, however. Shown in Figure 14 is a record of the envelope detector output, an agc signal-strength record, together with power spectral density plots of the envelope detector output signal at appropriate intervals.

Flame attenuation of P-band, but not of C-band, signals always occurs during the latter portion of stage-I operation [9]. The usual attenuation at P-band was observed on this test. No stage-I attenuation, however, was experienced at S , C , or X band, providing us with an upper bound for the ionization of the stage-I exhaust.

Diagnostic of flame attenuation is the cessation of attenuation that occurs at +256 seconds at stage-I shutdown. Shortly thereafter, at +257 seconds, the stage-II ignition flame causes an abrupt drop in signal strength, and an abrupt increase in the envelope fluctuations measured by the envelope detector. Note, however, that the large agc time constant used makes the drop seem slow on the agc record. The attenuation at the stage-II ignition flame is not confined to P-band. Abrupt drops in signal strength at stage-II ignition, lasting some 1 second, can be noted on S- , C-, and X-band records. This provides us with a lower bound for the electron density in the stage-II ignition flame. This is at least two orders of magnitude higher than the upper bound for the stage-I flame.

While stage-II ignition is simultaneous with stage-I shutdown, strictly speaking the stage-II ignition signal actuates a start cartridge which starts the turbo pump. Not until the discharge pressure of the turbo pump reaches 300 psi , however, are the main thrust chamber valves opened, starting actual stage-II combustion. This event is some one second after the stage-II ignition event, and is marked by an abrupt drop (staging notch) in the signal-strength records. The severity of the staging notch at stage-II ignition is aggravated by the fire-in-the-hole stage-I separation employed.

FIG. 14 POWER SPECTRAL DENSITY OF P-BAND AMPLITUDE FLUCTUATIONS DURING STAGE - I FLIGHT. UC - 13, 249.9 MHz PSD OF ENVELOPE DETECTOR OUTPUT

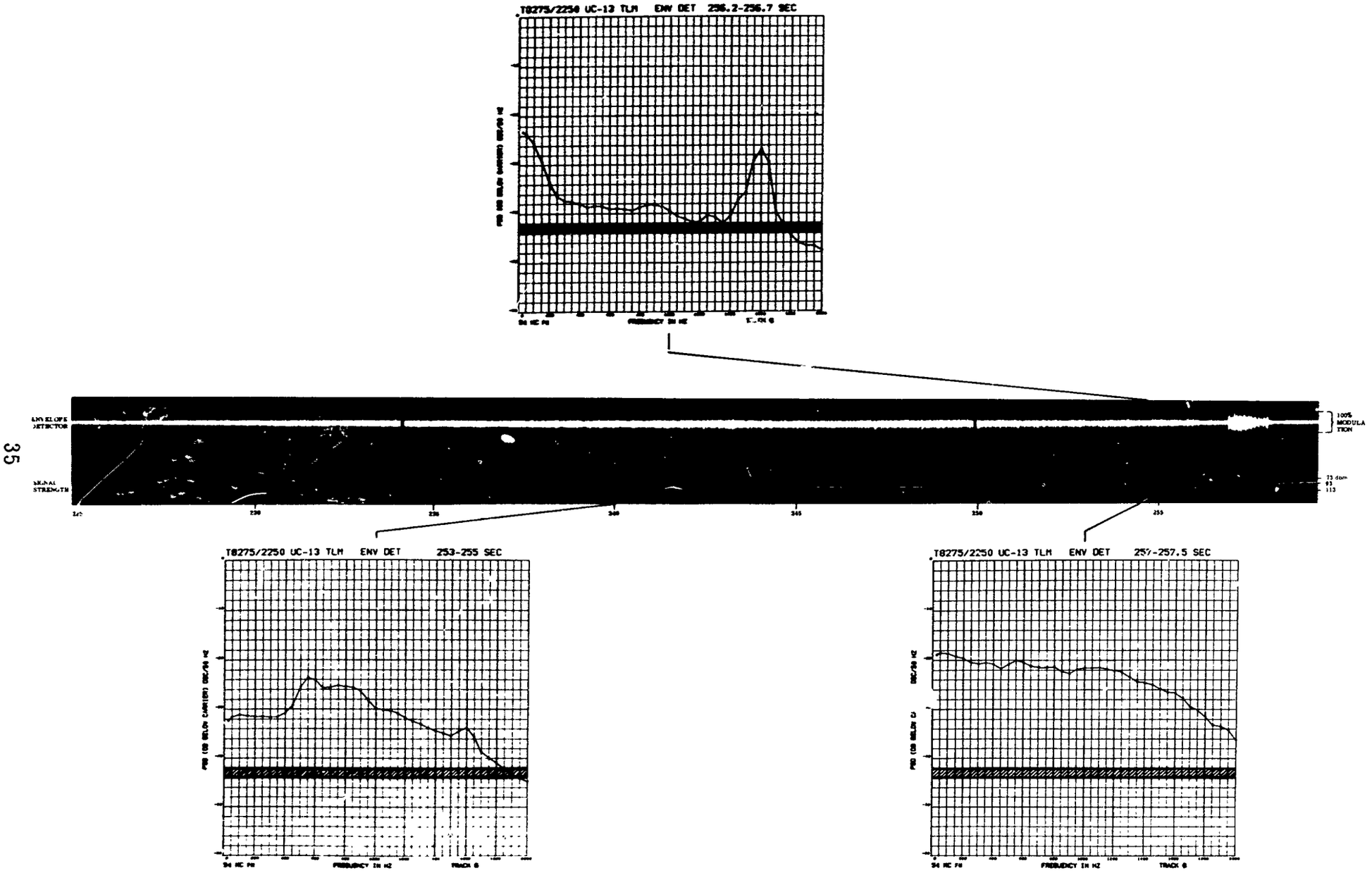

Stage I is actually separated by the exhaust of the stage-II engine. The exhaust flame of the stage-II engine is used to separate stage I. Until separation is accomplished, the stage-II exhaust flame exits through a series of blast portholes, which direct the exhaust transverse to the missile axis, surrounding the missile with flame. It is this flame that produces the high attenuation associated with stage-II ignition.

Power spectral density plots for the 253 - 255 (stage-I flame), 256.2 - 256.7 (no flame) and 257 - 257.5 second (stage-II ignition) periods are shown. The flat portion of the 257 - 257.5 plot at low frequencies is attributed to the combination of white noise (receiver front-end noise, appearing because of the low signal strength) and flame noise. The peak below 75 Hz in the 256.2 - 256.7 plot is due to hum and pickup. The peak at 1600 cycles is attributed to residual AM on the FM signal. The drop below 450 Hz in the 253 - 255 second PSD plot is unexplained.

F. PROBABILITY DENSITY

The signal amplitude fluctuations produced by the flame are random in nature and therefore, need to be described in statistical terms, i.e., power spectral density (PSD) and probability density. The power spectral density characteristics have been presented, it remains to present the probability density data. Since no phase noise data was obtained, our data is confined to the amplitude probability density, i.e., the probability that the amplitude fluctuation will have an amplitude between any two given amplitude values.

For each of the data spans analyzed in the preceding sections, a probability density and a cumulative probability analysis was conducted for the digitized data. The sampling and bandpass constraints used on the data were those already discussed in Section II B. Accordingly, our probability density and cumulative probability data is limited to amplitude fluctuations having frequencies in the range 20 - 1100 at X band, and 20 - 2000 Hz at S, C, and P bands. Computations were carried out on a 7094 digital computer using AFETR Computer Program Nos. 262 and 213.

The question of particular interest was, are the signal amplitude fluctuations produced by flame noise Gaussian, i.e., do they follow a normal probability density curve?

A convenient way to test whether a probability density function is Gaussian is to plot the cumulative probability (i.e. the integral of the probability density function) on normal probability paper. The scale of the paper has been stretched so that the cumulative probability plot will be a straight line if the distribution is normal (Gaussian). The degree of departure from a straight line is a measure of the departure of the distribution from a normal distribution.

Plots of the cumulative probability of flame-induced signal fluctuation during time segments already treated on preceding plots (Figures 2 - 7, and 13 - 14) indeed show that the probability density of the flame-induced signal amplitude fluctuations is Gaussian.

Typical plots of the cumulative probability of signal amplitude fluctuations induced by the zero-stage flame at X , S , and C bands on normal probability paper are shown in Figures 15 , 16 , and 17, respectively. It is evident that the data points lie very close to a straight line. The probability density function of zero-stage flame noise is, therefore, very close to normal. In Figure 18 the cumulative probability plot for signal amplitude fluctuations produced by the separation-rocket exhaust is shown, and in Figure 19 the plot for Stage-I, liquid propellant exhaust is shown. The distribution again is very nearly Gaussian, as correspondence to a straight line shows.

Cumulative probability plots show that fraction (in percent) of the amplitudes having a value less than that indicated by the abscissa. To illustrate the use of the cumulative probability plots, as well as to illustrate that the flame noise amplitude distribution is normal (Gaussian), consider the question, what fraction of the amplitudes lie within one sigma (σ) of the mean amplitude. For a normal distribution, this is 68%.

Referring to Figure 15, we read that 0.84% of the amplitudes are less than $\mu + \sigma$ (0.04 + 0.43) and that 15% are less than $\mu - \sigma$ (0 - 0.43) where μ is the mean, and σ is the standard deviation. Subtracting gives us the fraction lying within one sigma (σ) of the mean, or

FIG. 15 PLOT OF CUMULATIVE PROBABILITY OF X-BAND ENVELOPE FLUCTUATIONS ON NORMAL PROBABILITY PAPER UC-2
109.5 - 111.5 SECONDS, ZERO-STAGE EXHAUST

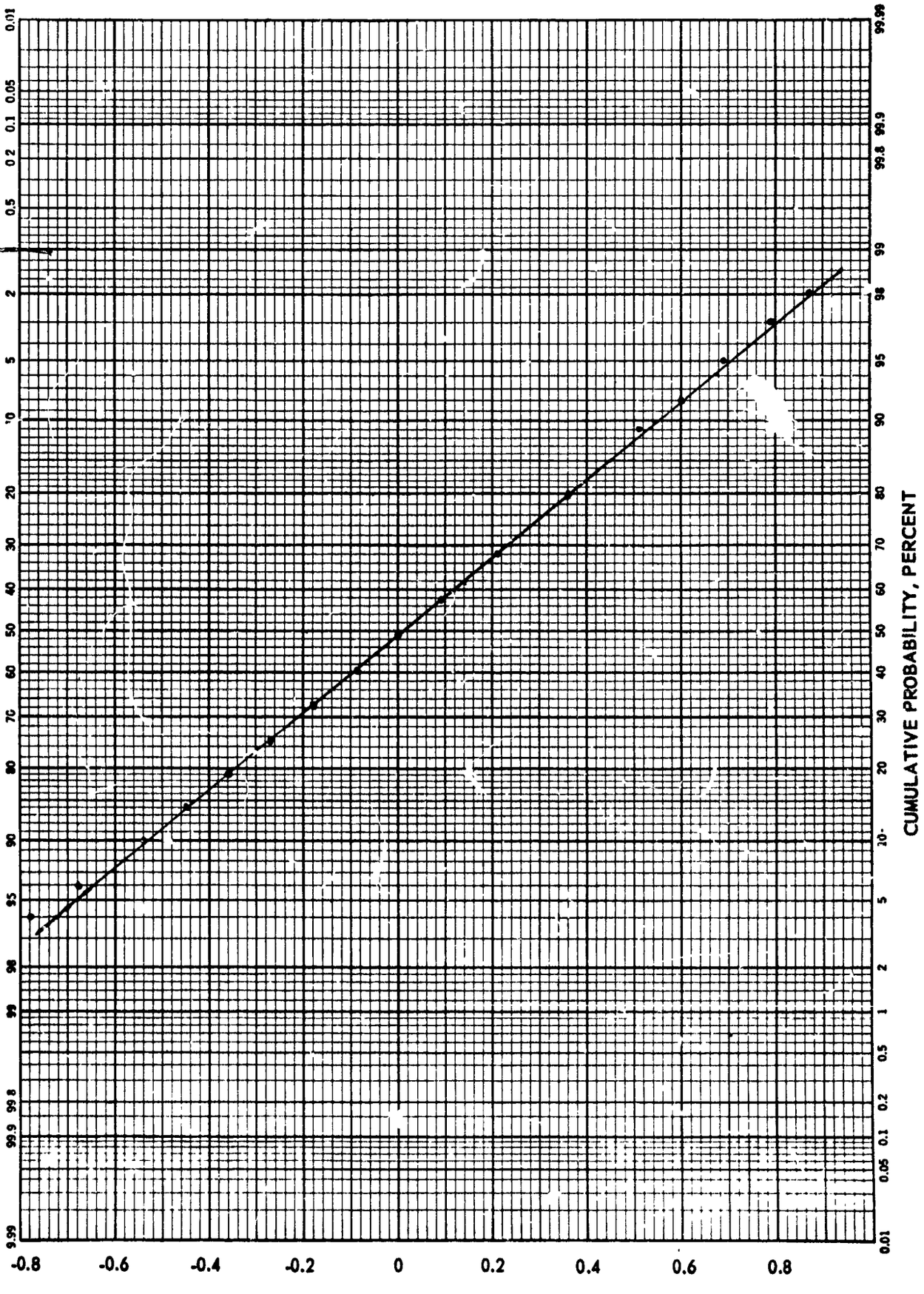

μ = 0.04

σ = 0.43

FIG. 16 PLOT OF CUMULATIVE PROBABILITY OF S-BAND ENVELOPE FLUCTUATIONS ON NORMAL PROBABILITY PAPER UC-11 108-110 SECONDS, ZERO-STAGE EXHAUST

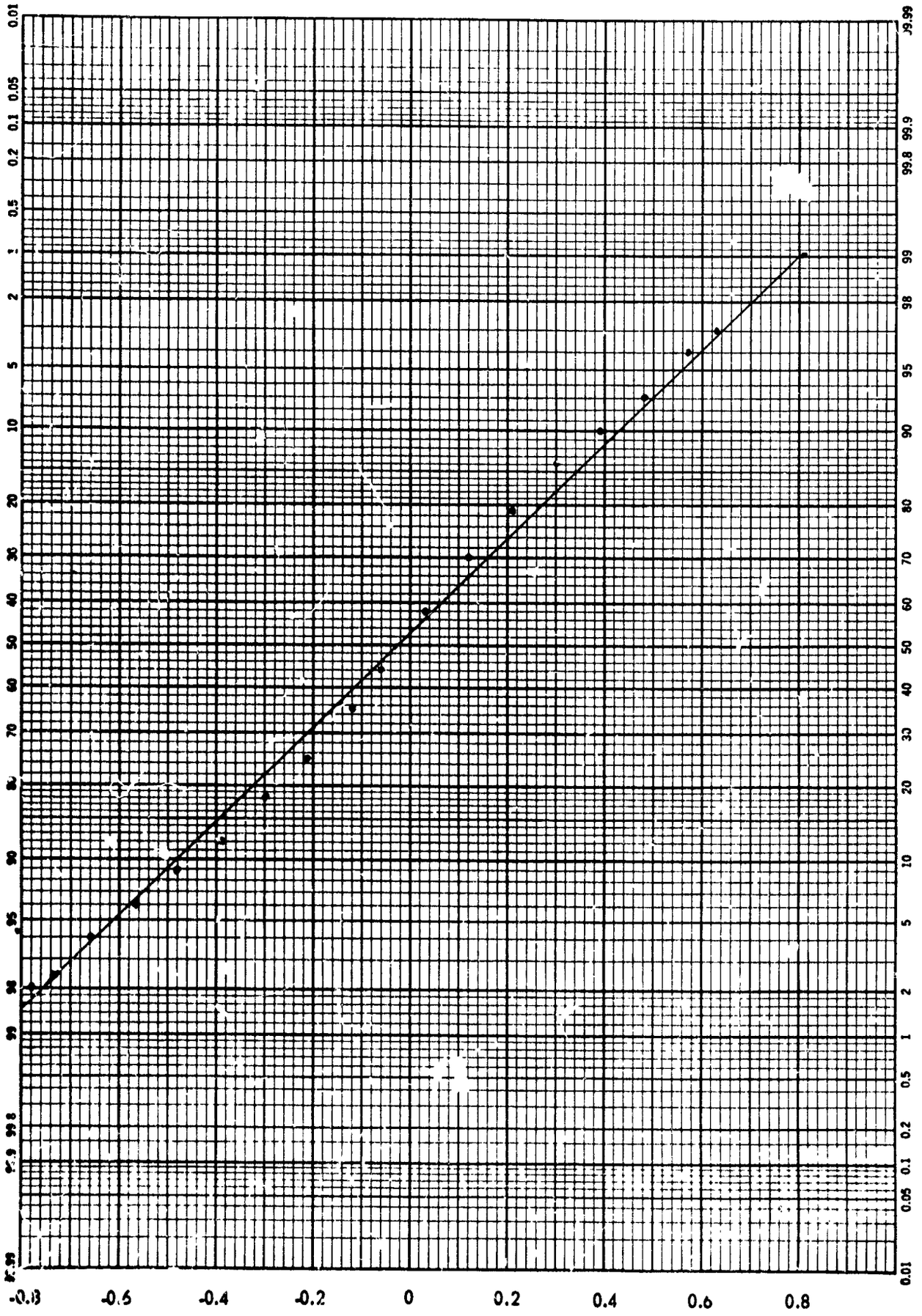

FIG. 17 PLOT OF CUMULATIVE PROBABILITY OF C-BAND ENVELOPE FLUCTUATIONS ON NORMAL PROBABILITY PAPER UC-13
112.1 - 112.5 SECONDS, ZERO-STAGE EXHAUST

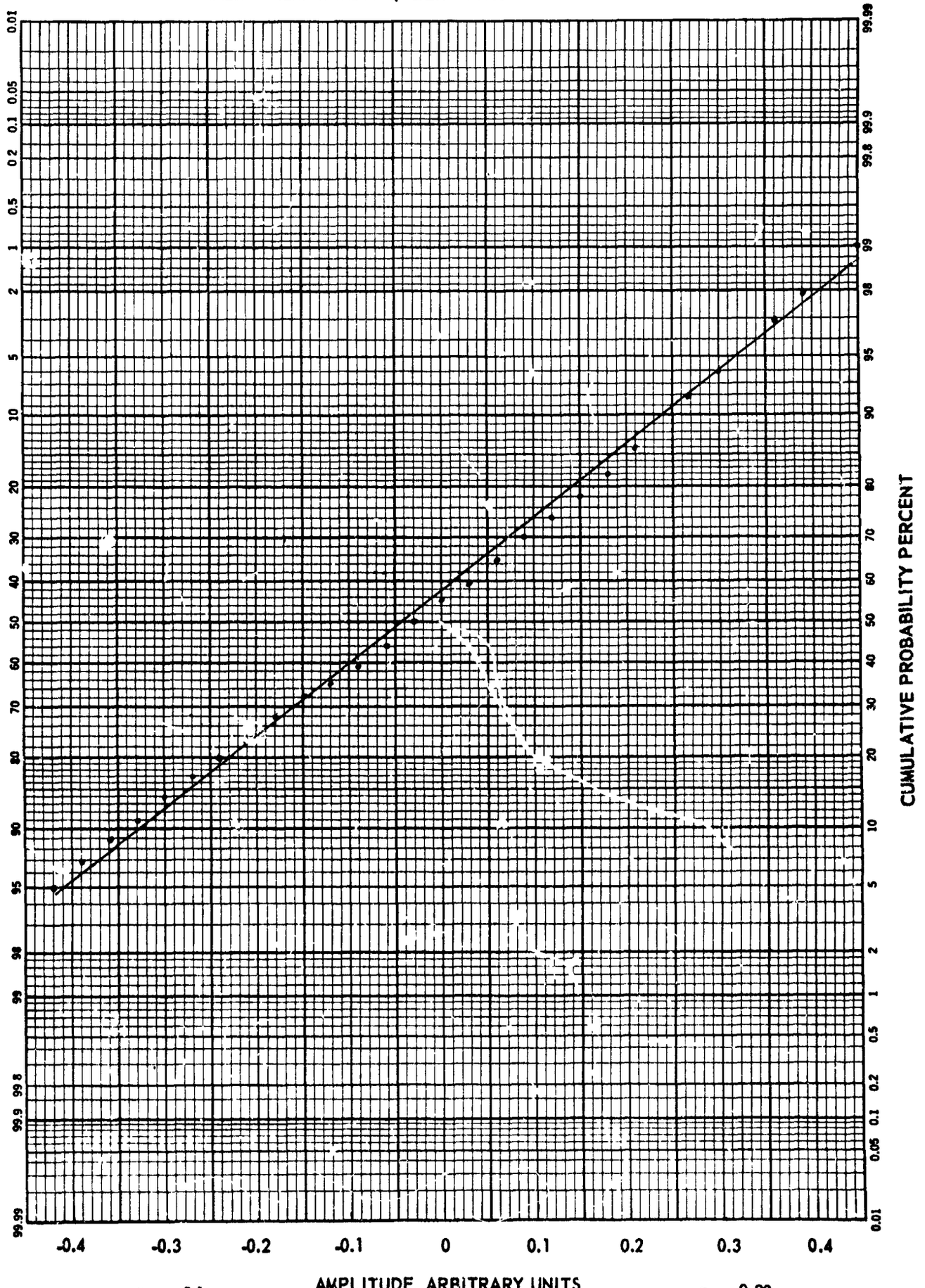

FIG. 18 PLOT OF CUMULATIVE PROBABILITY OF X-BAND ENVELOPE FLUCTUATIONS ON NORMAL PROBABILITY PAPER UC-2
121-122 SECONDS, SEPARATION-ROCKET EXHAUST

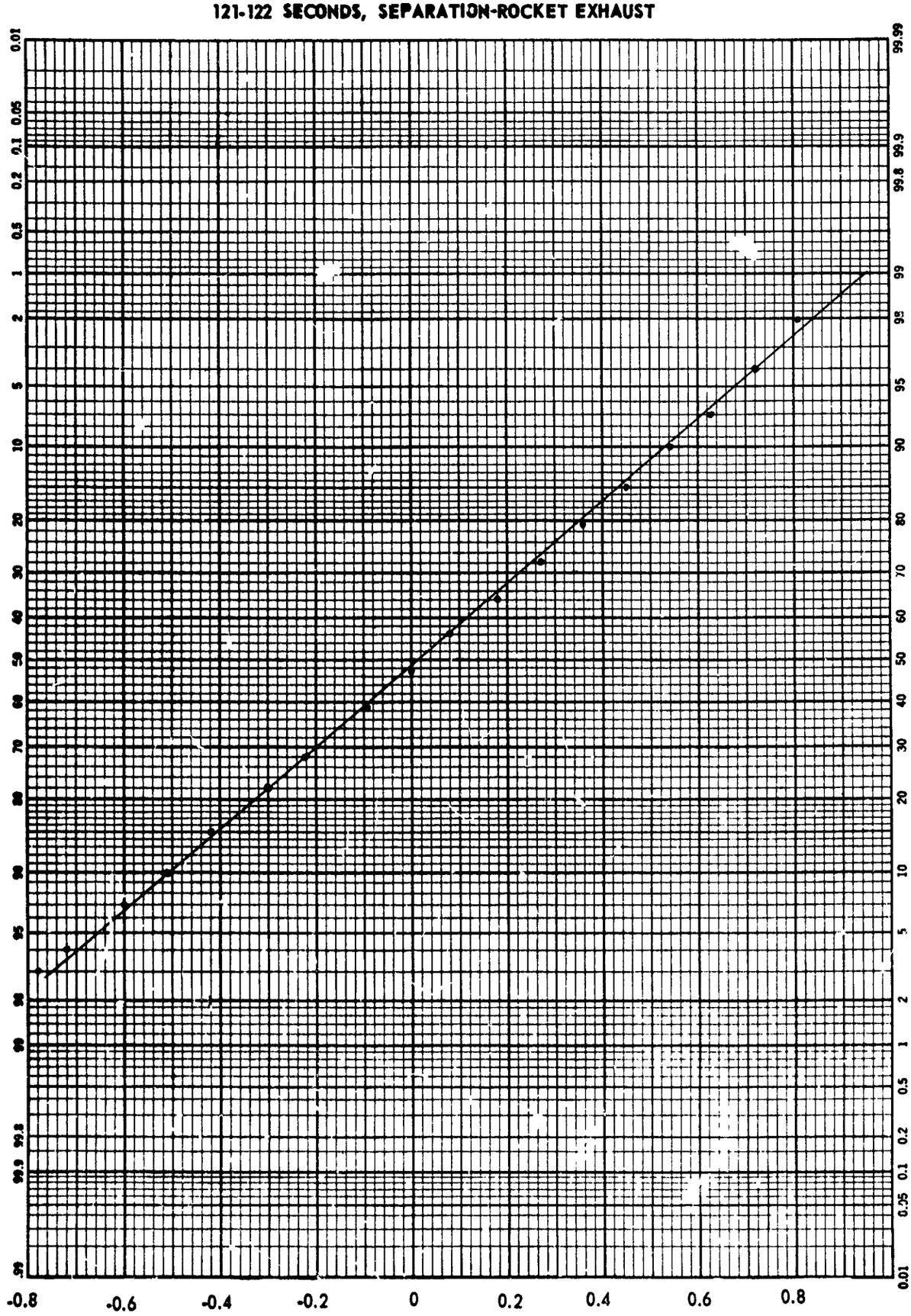

FIG. 19 PLOT OF CUMULATIVE PROBABILITY OF P-BAND ENVELOPE FLUCTUATIONS ON NORMAL PROBABILITY PAPER UC-11
252.1 - 252.1 SECONDS, STAGE I EXHAUST

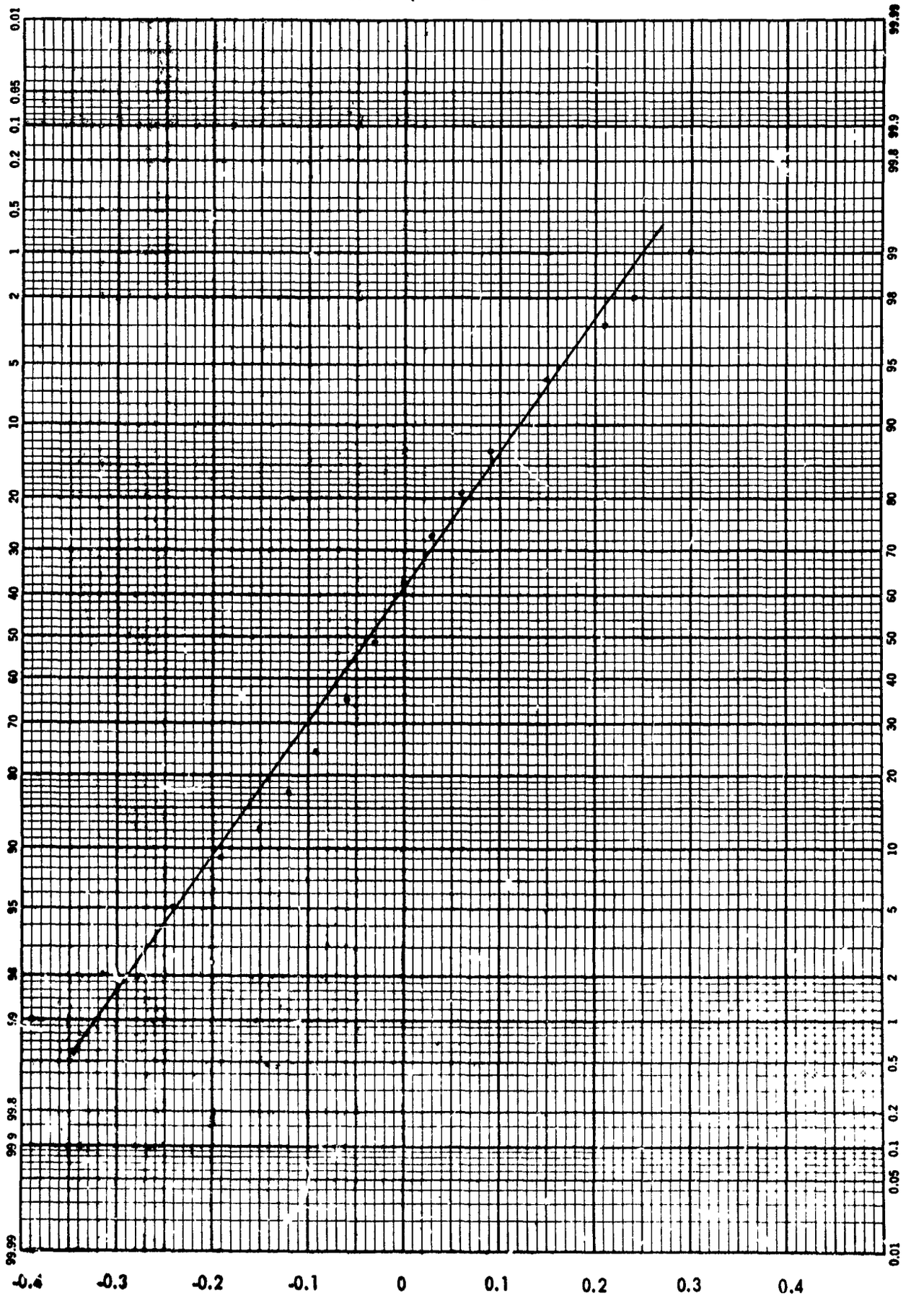

69%. This is sufficiently close to the 68% characteristic of a normal distribution. As our cumulative probability plots of Figures 15 - 19 show, the signal amplitude fluctuations produced by flame noise have a probability density function that is very nearly Gaussian.

III. SPECIAL TOPICS

A. EXHAUST PLUME INTERFERENCE WITH PULSE TRANSMISSION

While the transmission of pulses through laboratory-generated plasmas has been treated in the literature [10], no published data on pulse transmission through in-flight rocket exhaust plumes has appeared. Of particular interest is the question whether the rocket exhaust plume behaves as a dispersive medium, i.e., whether the rocket exhaust plume would modify the pulse shape as would a dispersive medium [11]. For these reasons, instrumentation was set up to measure received pulse shape at three sites (UC-2, UC-11, and UC-13).

Free running Dumont Type 321A cameras were used to photograph the received pulse displayed on Tetronix oscilloscopes. While it was desired to photograph every pulse, a compromise had to be reached between conflicting requirements of a limited camera film capacity (480 feet, 35 mm film), a minimum time span to be covered (280 seconds), a minimum acceptable separation of individual pulse traces, and a maximum film speed (3600 in./min.). In order to cover the required time span, it was only possible to photograph every 22nd pulse of the 2200 prf pulse repetition frequency at the 1200 in./min. film speed that was used. A gating circuit, activated by the standard 100 pps timing circuit, was used. The timing impulses were used to open the gate. The next pulse coming along after the gate was opened triggered the sweep. Use of the common 100 pps timing impulses to gate the oscilloscopes made it possible to observe the same 22nd pulse at each site. Timing was provided by a timing light built into the camera, but separated from the film gate by one inch of film travel.

Satisfactory photographs of pulse wave shapes, showing the effects of rocket exhaust interference were obtained at three sites, UC-2, UC-11, and UC-13.

1. Pulse Data At UC-2

The UC-2 site was located just outside the attenuating region of the zero-stage flame. Nevertheless, flame interference with pulse transmission was evident.

Pulse shapes recorded at the UC-2 site are shown in Figure 20 for zero-stage flame, separation-rocket flame, and for no-flame periods. Also shown is a reproduction of the pulse amplitude fluctuations as obtained from the output of a boxcar demodulator.

During the no-flame period at + 120 seconds a uniform succession of pulses of equal amplitude is recorded.

At UC-2 no flame attenuation was evidenced because the site was outside the attenuation zone of the zero-stage flame (minimum aspect angle, 18 degrees). Nevertheless, flame noise was evident at this site. This flame noise evidences itself by changes in the pulse amplitude, as shown in the 96.5 second segment.

The separation-rocket exhaust produced appreciable attenuation (10 db) and severe noise. The effect on the pulse shape is indicated in the 121.6 and 122.2-second time strips. Again flame interference manifests itself by randomly changing the pulse amplitude. Also evident are blank pulses. Blank pulses result from a pulse level below the level required to trigger the sweep (1/10 normal pulse height). Flat pulses, as shown at 121.6 seconds were occasionally seen. As will be shown later in Figure 22, these pulse shapes were not attributable to flame interaction.

Flat pulses such as shown on the 121.6-second and on the 122.2-second records were caused either by (1) blocking of the receiver, or (2) transmission of an abnormal pulse by the transmitter. Illustrations of (2) will be given in Figure 22.

The agc time constant employed on this test was long relative to the 2200 prf pulse repetition rate. A succession of highly-attenuated pulses will cause the agc to open up to the maximum gain of the receiver. The next normal pulse coming along will block the receiver, as illustrated

FIG. 20 ZERO - STAGE AND SEPARATION - ROCKET EXHAUST INTERFERENCE WITH PULSE TRANSMISSION 9100 MHz, 1/2 MICROSECOND, 2200 PRF, UC - 2

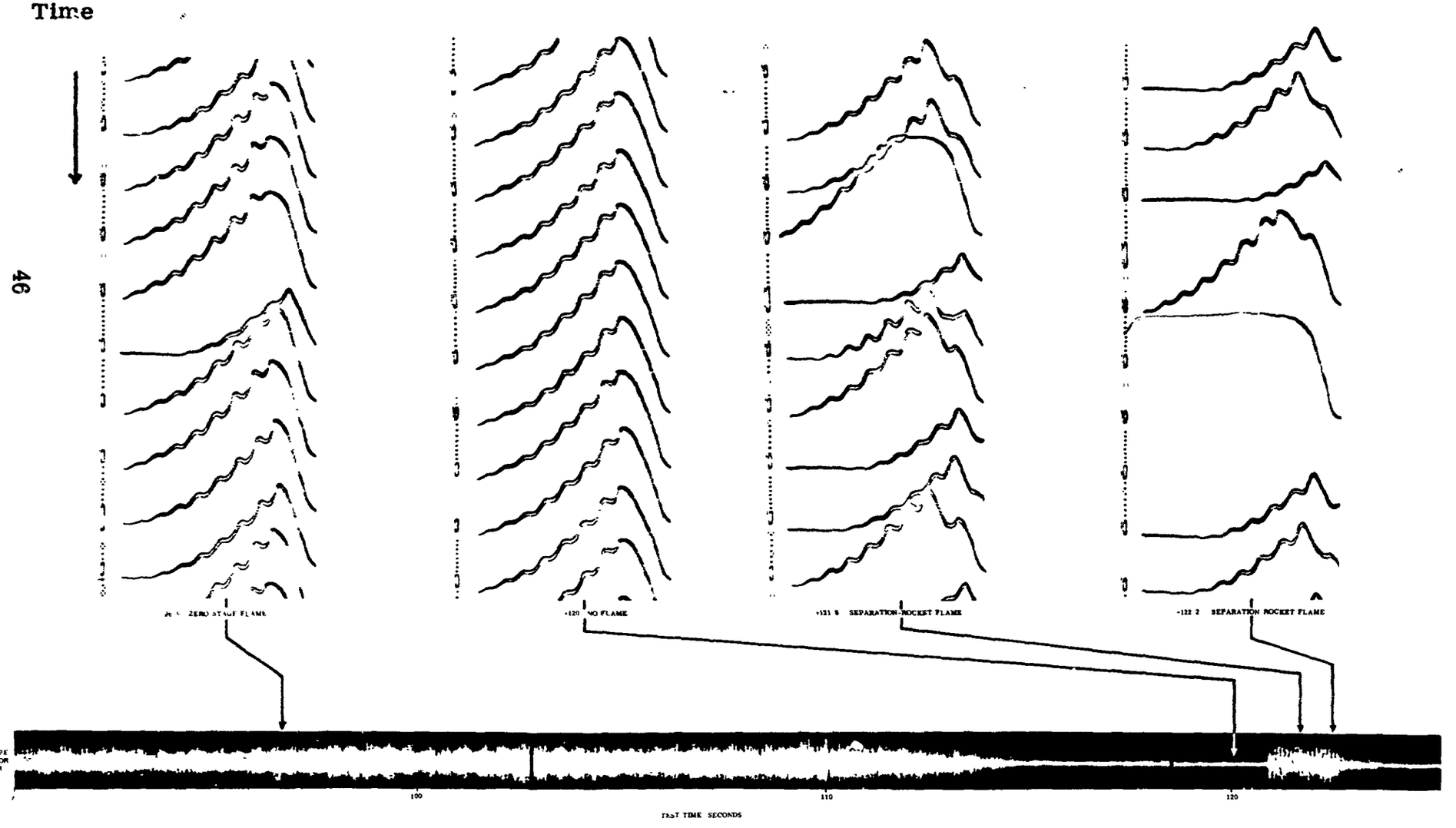

by the fifth pulse on the 122.2-second record. Here the receiver is blocked (saturated) for several times the pulse length.

Unfortunately the series of highly-attenuated pulses that preceded the fifth pulse are not visible because only every 22nd pulse was photographed. The records presented show timing dots. Small dots recur at a 1 millisecond spacing; dashes recur at 10 millisecond intervals. Increasing time runs from the top to the bottom of the record.

In order to further explore receiver blocking as well as to better visualize the range of amplitude fluctuations, we propose to add a standard, gated motion picture camera on the next test. Each frame will give us a superposition of a large number of pulses. Not only will the maximum and minimum pulse heights be visible, but film density will give an approximate distribution of pulse amplitude heights.

2. Pulse Data at UC-13

Pulse data at UC-13 was of considerable interest because of the location of UC-13 deep in the flame-attenuation region.

The pulse shapes recorded at UC-13 are shown in Figure 21. As before, the no-flame period (+113.5 seconds) shows a uniform succession of pulses of equal amplitude.

Zero-stage flame effects are shown in the recorded 106-second segment. The average attenuation at this time is < 40 db, and the aspect angle is 5 degrees. As observed at UC-2, flame interference manifests itself only by varying the amplitude of the pulse. Missing pulses result from flame decrease of pulse amplitude below the trigger level. No pulse distortion or stretching can be observed.

Attenuation and flame noise decreases as the thrust decays. The 113.5 second segment corresponds to the thrust-decay period. (See Figure 23 for actual thrust-decay characteristics.) Flame interference is decreased, as expected.

Superimposed on the pulse in Figures 20, 21, and 22 is an unwanted damped oscillation with its typical decay. This transient originates in the video amplifier and is shock excited by each pulse.

FIG. 21 ZERO - STAGE EXHAUST INTERFERENCE WITH PULSE TRANSMISSION
9100 MHz, 1/2 MICROSECOND, UC - 13.
SITE UC - 13 DEEP IN FLAME ZONE

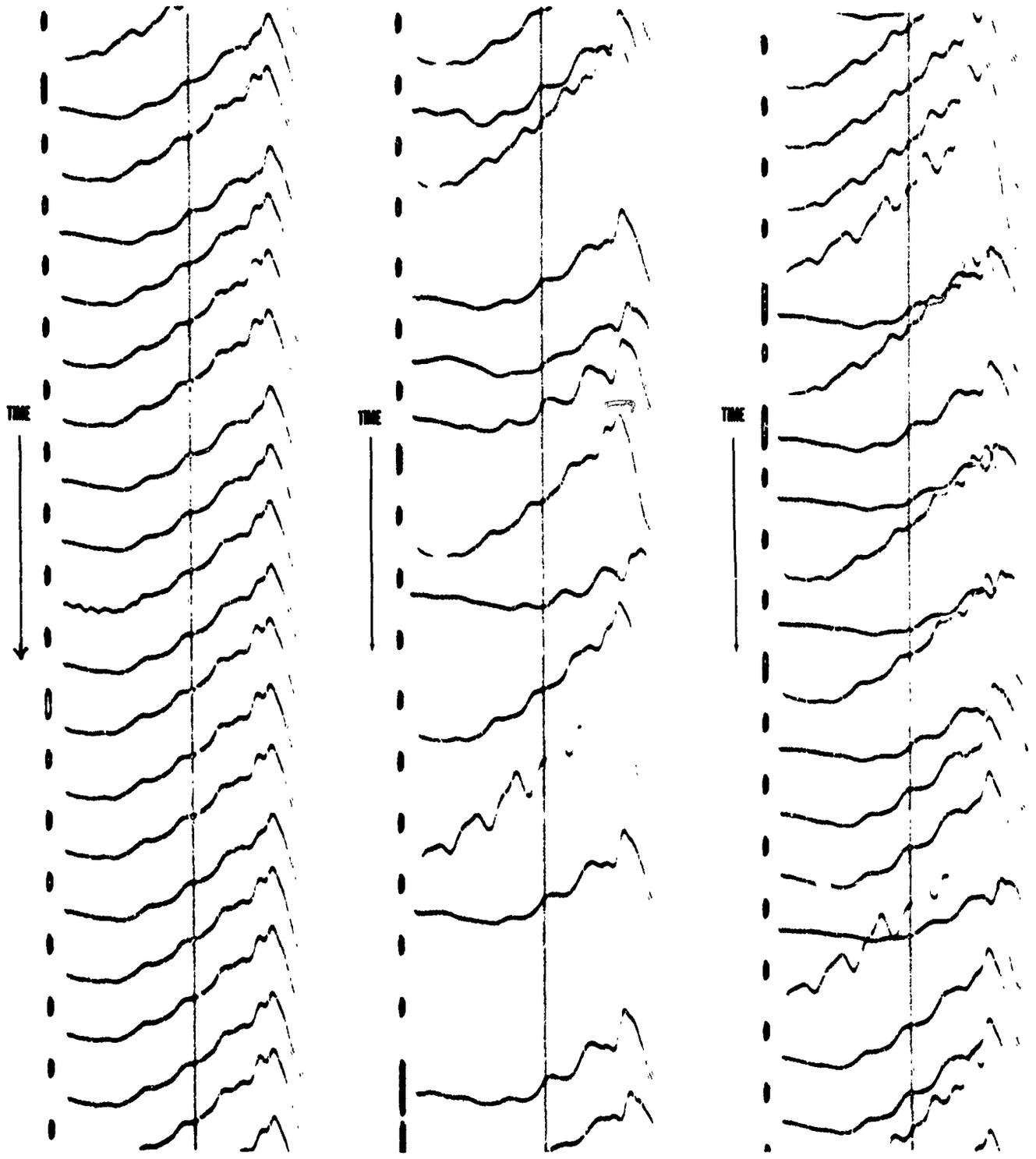

NO FLAME 113.6 SECONDS

ZERO - STAGE FLAME 106 SECONDS
(ASPECT ANGLE - 5 °)

THRUST DECAY 113.5 SECONDS
(ASPECT ANGLE - 6 °)

3. Abnormal Pulse Shapes

Abnormally-flattened pulse shapes aroused interest and raised the question, does the flame behave as a dispersive medium? Some flattened pulses were caused by receiver blocking, as already discussed in Section III A 1. For the others, a close examination of records showed the same pulse to occur at the same time at a second site (UC-2) that was outside the flame attenuation zone. Two examples, one at 104.8 and the other at 114.1 seconds are shown in Figure 22. While a 0.01 second displacement appears in the time occurence at the two sites, this interval was noted to be consistent for all the flattened pulses observed. At 1200 in/min, a 0.01 second displacement is readily explained by a 0.2 inch displacement of the trace relative to the timing light. The simultaneous occurence of flat pulses at sites within and without the attenuating flame zone permit us to conclude that these occasionally-flattened pulses are caused by the transmitter, not by the flame.

No pulse distortion by the rocket exhaust plume was observed on this test. We can conclude that the exhaust plasma does not behave as a dispersive medium. The exhaust plume serves to attenuate the pulse amplitude in a random manner, but does not affect the pulse shape otherwise. Interaction with the receiver agc can serve to increase the amplitude of a pulse when following a series of attenuated or missing pulses.

B. THRUST DECAY

The relation of thrust decay to recovery from attenuation has been discussed in an earlier report [7]. Observation of the behavior of the signal strength is a useful tool for evaluation of the degree of flame attenuation and helps to identify loss in signal strength as flame attenuation, removing doubts as to other possible causes, such as antenna pattern, nulls, cross polarization, or loss of track. If flame attenuation is present, a recovery from attenuation will be observed as the thrust decays. Where there is no recovery in signal strength as the thrust decays, one cannot say there is flame attenuation.

FIG. 22 X - BAND PULSE SHAPES.

SIMULTANEOUS RECEPTION AT UC - 2 AND UC - 11 SITES

9100 MHz , 1/2 MICROSECOND

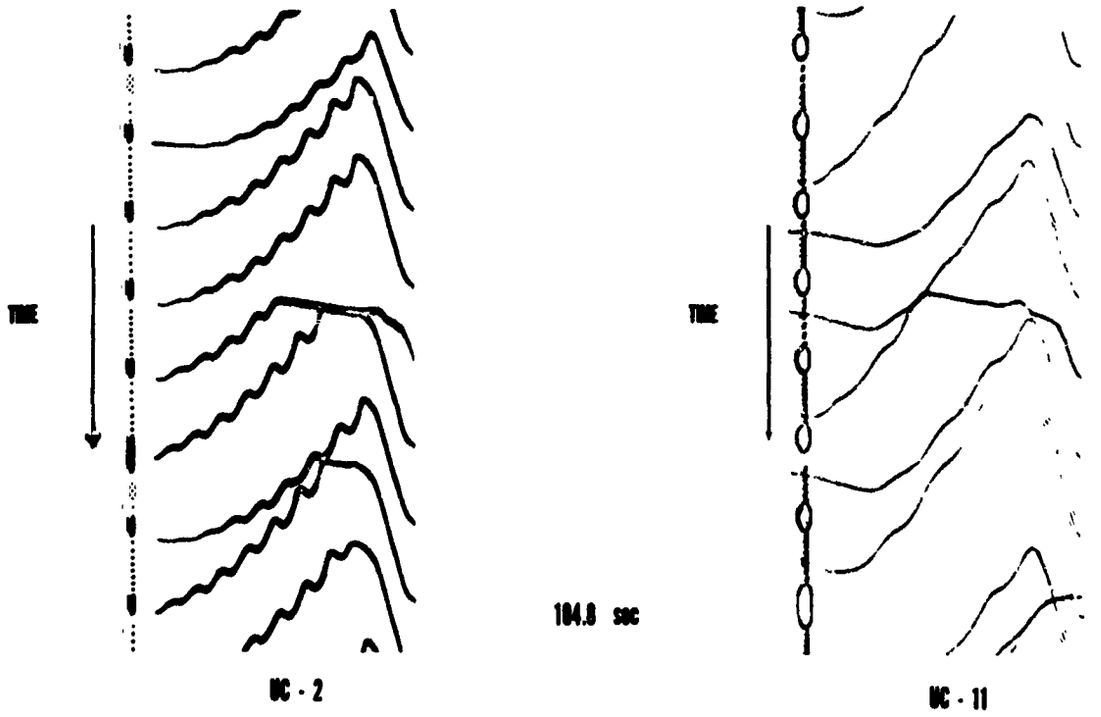

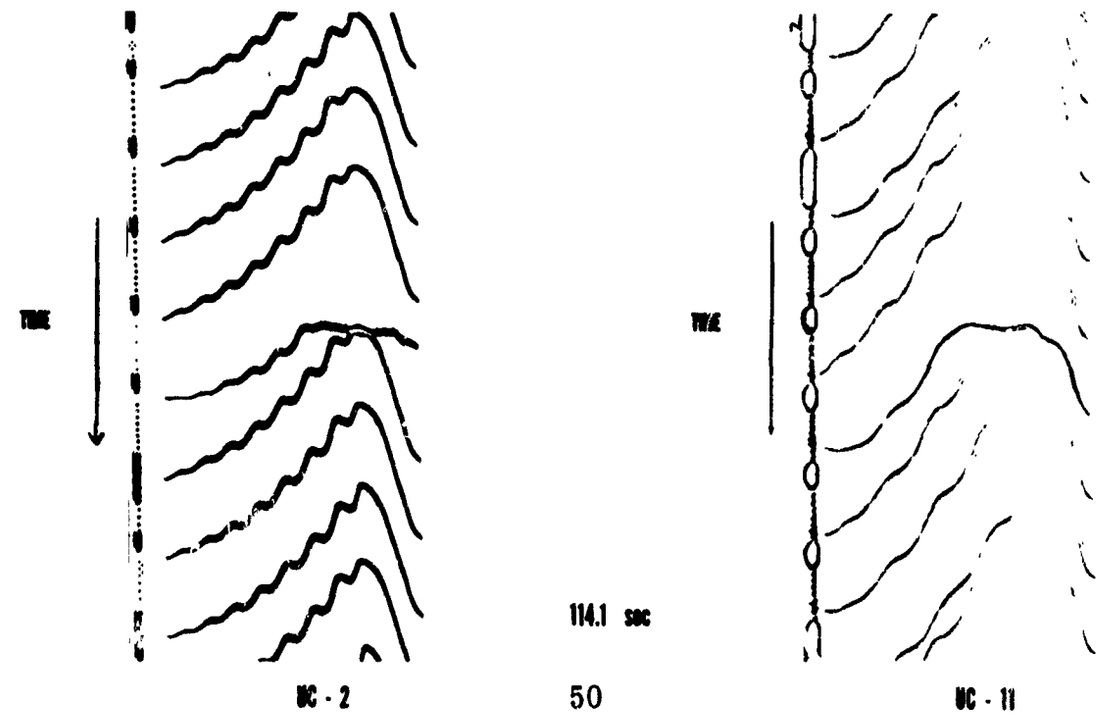

The telemetered thrust-decay characteristic of the zero stage on Test 8275/2250 is shown in Figure 23. The decay is sudden. The thrust has decayed to approximately 40% of its value at T+110 seconds. Reference to signal-strength records of X-band signal strength at UC-13 and the 19.1 radar, Figures 8 and 9, respectively, of the companion report [1] provide excellent illustrations of the correlation of thrust with attenuation.

Whereas flame attenuation ceases abruptly as the thrust decays, the data taken on Titan IIIC clearly show that flame noise continues for some three seconds after the thrust reaches its 40% value. (See Figures 28, 29, and 30 presented in Section III E.) Flame noise continues until the thrust decays to some 25% of its value and extends to periods where the attenuation is less than 3 db.

C. SODIUM AND POTASSIUM IMPURITY MEASUREMENTS

1. Background

While it is generally acknowledged that alkali-metal impurities are the primary cause of rocket exhaust ionization, no published measurements are available as to the alkali-impurity content of the Titan IIIC zero-stage and separation-rocket propellants. For this reason we have undertaken to measure the alkali impurity content of the Titan IIIC propellants, in particular, sodium and potassium.

Alkali-metal impurity contents of samples of the zero-stage and separation-rocket propellant furnished by the United Technology Corporation (UTC) were analyzed by the Air Force Chemical Laboratory at the Air Force Eastern Test Range. The alkali-metal impurities are measured by an atomic absorption spectrophotometer, using double-distilled water. As a check, both the water itself and the water used to wash the sampling containers are analyzed for sodium and potassium. The detection limit of the absorption spectrophotometer is 0.1 ppm K and 0.1 ppm Na. Sufficient outside volume of the solid propellant samples are cut away under chemically controlled conditions. Several different samples from the interior of the propellant sample are analyzed. The propellant is first burned in a bomb calorimeter. The residue is then washed with double-distilled water, and the wash water is analyzed in the spectrophotometer.

FIG. 23 ZERO-STAGE TELEMETERED THRUST DECAY CHARACTERISTIC
TEST 8275/2250 SRM I

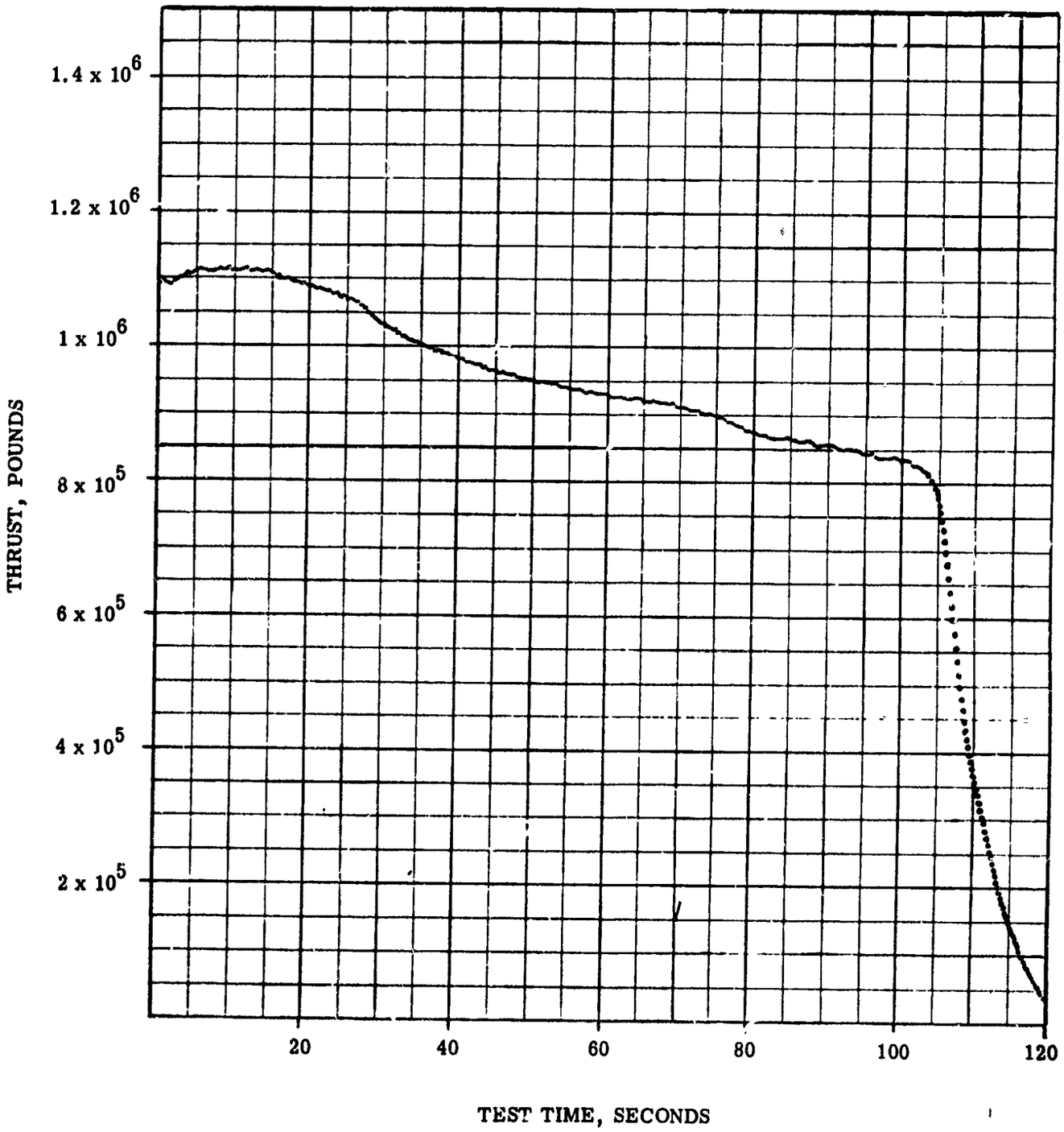

3. Results of Alkali Impurity Measurement, Zero-Stage and Separation Rocket Propellants

Samples of zero-stage and separation-rocket propellant were received from UTC in June 1966 and June 1967. While these samples are said by UTC to be typical of current propellants, no information could be obtained that would link these samples with a particular Titan IIIC vehicle.

The results of the Air Force Chemical Laboratory analysis of these propellant samples are given in Table I.

TABLE I
ALKALI IMPURITY CONTENT MEASUREMENTS
TITAN IIIC ZERO-STAGE AND SEPARATION
ROCKET PROPELLANTS

Propellant	Date of Analysis	Alkali-Metal Impurity Content	
		Na ppm	K ppm
Zero-Stage	6 - 20 - 66	62	65
	6 - 19 - 67	380	360
Separation Rocket	6 - 20 - 66	53	52
	6 - 19 - 67	61	30

While single entries are shown in the table, each entry represents the average of several analyses. In practice, several small pieces were taken from the interior of each propellant sample supplied. The small pieces were analyzed separately and the average of these results have been entered in the table.

Fifty parts per million of potassium or of sodium impurity can cause severe flame attenuation. It is a level often found in solid propellants which have no specifications limit on alkali-metal impurities.

The 360 ppm of potassium and 380 ppm of sodium is some seven times the value usually reported for solid propellants and represents a very high level as far as flame attenuation is concerned.

While an earlier sample, analyzed June 20, 1966 showed levels of only 60 ppm, this more-normal level fails to be a source of comfort since since (1) Mr. Richard Hough of UTC informs us that the 1967 sample is likely to be more representative of Titan IIIC zero-stage propellant than the 1966 sample, and (2) investigation of the source of the alkali-metal impurities indicates that a value of 350 ppm, or higher, is to be expected.

4. Ammonium Perchlorate - Source of Sodium and Potassium Impurities

The prime contributor to alkali-metal impurity in solid propellants is known to be ammonium perchlorate [12]. The sodium and alkali-metal impurities originate in the rock salt (NaCl), which is the starting point in the manufacture of ammonium perchlorate. Potassium is the more difficult impurity to eliminate. Because of its low ionization potential (4.32), potassium is many times* as effective in producing the free electrons which cause the exhaust attenuation than is sodium (5.12 ev.).

---

* Calculation of the fractional ionization X_K of potassium and X_{Na} of sodium by the Saha equation illustrates the strong dependence on temperature T, as well as the increased ionization of potassium, i.e., $X_K / X_{Na} = 8, 10, 22$ for $T = 2250, 2000, 1500^{\circ}$ K, respectively. For a specific propellant system, however, calculation of the increased ionization of potassium impurity requires a detailed examination of the ionic-chemical kinetics of the flow from the combustion chamber to the exit plane, not only to determine the temperature at which the ionization can be considered frozen, but also to include the action of chemical (e.g., $K + OH \rightleftarrows KOH$) as well as electron (e.g. $Cl + e \rightleftarrows Cl^-$) sinks. Further, the increased ionization of potassium (ratio X_K / X_{Na}) can be expected to be different for afterburning phenomena, where the temperature T and the action of chemical and electron sinks can be expected to differ.

In an effort to shed light on the high values of sodium and potassium content (380, and 360 ppm) obtained in the AFETR analysis of the zero-stage propellant supplied to us by UTC, we contacted the Pacific Engineering and Production Co. of Nevada, the source of the ammonium perchlorate, which makes up 72% of the composite zero-stage propellant. We were informed in writing [13] that the control analysis of the production of regular type ammonium perchlorate indicates a combined sodium and potassium content of 600 to 800 ppm.

Considering the information supplied by the Pacific Engineering Company of Nevada, together with the fact that ammonium perchlorate makes up 72% of the zero-stage propellant, our measured values of 360 ppm of potassium and 380 ppm of sodium seem to be quite reasonable.

As a further check on the alkali-impurity content, we have requested additional samples of zero-stage and separation-rocket propellant for alkali impurity analysis. We plan to continue to measure the alkali-impurity content for at least several additional tests.

For reference, the composition by weight of the zero-stage propellant as given from the Ordnance Device Data Sheet, ETR-UTC-64-101 is:

Ammonium Perchlorate	72%
Aluminum Powder	10%
PBAN	10%
Additives	8%

5. Results of Alkali-Impurity Measurement, Stage I Liquid Propellants

An analysis of the alkali-metal impurity content was also conducted on the liquid propellants used in Stage I. Samples for the analysis were drawn from the Complex 41, the fill and drain line. The results of the analysis of the Aerozine-50 fuel, and the nitrogen tetroxide oxidizer are shown in Table II.

TABLE II

MEASURED ALKALI-METAL IMPURITY LEVELS

TITAN IIIC STAGE-I PROPELLANT

Propellant	Alkali-Metal Impurity Content, ppm Na	K	Date
Aerozine-50	0.013	< 0.01	6-8-66
	---	< 0.01	6-14-66
	0.04 0.02	< 0.01	6-20-67
Nitrogen Tetroxide	0.01	0.01	6-8-66
	0.01	0.01	6-14-66
	0.02	< 0.01	6-20-67

The alkali-metal impurity content of the liquid propellants of stage I are seen to be several orders of magnitude lower than that of of the solid propellant. This is the reason for the lower ionization (hence lower attenuation) of the liquid stage I.

6. Alleviation of WTR Attenuation Problems by Control of Alkali Metal Impurities in the Zero-Stage Propellant

The data presented in this report indicates that AFWTR can expect to experience serious instrumentation problems at X- and S-bands for aspect angles to the roll axis less than 16 degrees. The report of Phelps [14], in fact, points to aspect angles much lower than 16 degrees. Necessary redesign or relocation of established WTR instrumentation so as to operate in the Titan III flame environment may conceivably entail costly expenditures.

We wish to call attention to a means of alleviating the zero-stage flame interference problem - that is to control the offending alkali-metal impurities (potassium and sodium) by placing tight limits on the potassium and sodium content of the ammonium perchlorate used in the manufacture of the zero-stage propellant. This approach is already being applied for tactical missiles which have a tight specification on the allowable potassium and sodium content of ammonium perchlorate. The alkali-metal impurity content can be, and is, controlled to limit the degree of flame attenuation. It is worthy of note that Aerojet-General monitors the alkali impurity content of lots of ammonium perchlorate it receives from American Potash, and selects those lots with the lowest alkali-metal impurity content for propellants for which a specification of maximum allowable attenuation has been set by the user [12]. In this manner, alkali-metal contents of as low as 10 ppm of sodium and of potassium are achieved, in contrast to the more usual 50-100 ppm. Conversely, those propellants for which no specification for maximum allowable attenuation have been set are fabricated by Aerojet General with the higher alkali-impurity content lots of ammonium perchlorate, thus yielding a higher level of alkali-metal impurity by negative selection.

Correspondence from both Pacific Engineering and Production Company of Nevada [13] and from American Potash and Chemical Corporation [15] informs us that ammonium perchlorate can be furnished with alkali-metal impurity levels of as low as 25 ppm potassium and 25 ppm sodium. This is over a 10-fold reduction in the level of these impurities

in the ammonium perchlorate currently supplied by Pacific Engineering and used in the Titan IIIC zero-stage propellant.

Such a 10-fold reduction in sodium and in potassium content can be expected to yield a 3 to 1 reduction in the electron density. In accordance with the empirical exhaust plume model presented in Section III D, a 3 to 1 reduction in electron density will yield a 3 to 1 reduction in the number of decibels of attenuation. That is, 30 decibels of attenuation (at X , C, S, or P band) would be reduced to 10 decibels.

The reduction in attenuation that can be achieved by the use of the above mentioned 25 ppm low-alkali ammonium perchlorate in solid propellant formulation is currently being tested in an altitude-simulating facility by Dr. L. Douglas Smoot, Associate Professor, Chemical Engineering Department, Brigham Young University, Provo, Utah.

The cost increase of the low-alkali-content ammonium perchlorate (25 ppm Na, 25 ppm K) must be weighed against the possible cost of re-designing and/or relocating WTR instrumentation. American Potash writes [15] that ammonium perchlorate with only 25 ppm Na and 25 ppm K impurity can be supplied at 2 to 3 times the cost of regular Class I material. In carload lots, this would mean an increase from 20 cents per pound to 40 to 60 cents per pound. Pacific Engineering writes [13] that the price increase would probably fall in the range 3 to 5 times the price of ordinary materials. However, in lots of 10^6 pounds (as would be required for Titan III missiles), we were informed by Mr. J. W. Jenney, Manager of Market Development and Technical Services, West, American Potash and Chemical Corporation, that 25 ppm low-alkali ammonium perchlorate might be supplied at an additional cost of only 5 cents per pound.

Reflected in terms of the five-segment Titan III solid motors the additional cost for the 10-fold lower alkali-impurity ammonium perchlorate could be \$0.05 (0.72)(840,000) or \$30,000 extra for both motors of the zero stage. For the seven-segment Titan III motor, this could be (7/5) 30,000 or \$42,000 extra for both zero-stage motors.

We, therefore, strongly recommend that the use of ammonium perchlorate with a maximum limit of 25 ppm sodium and 25 ppm potassium be given careful consideration and thoroughly explored in the solution of AFWTR Titan III flame problems before expensive instrumentation relocation or addition is undertaken. In any case it would seem essential to impose some realistic limit on the allowable alkali-metal impurity content. Present levels of 350 ppm are unreasonably high, and could actually go higher since no specification [16] on the amount of sodium or potassium impurity of ammonium perchlorate used in Titan IIIC missiles currently exists.

D. EXHAUST PLUME IONIZATION MODELS

The attenuation of RF signals to and from the missile is determined by the frequency f, the distribution of the electron density N, and the collision frequency (electron collision frequency for momentum transfer) ν throughout the exhaust plume. Given a model of the distribution of the electron density N and collision frequency ν (contours of constant N and constant ν) one can compute the attenuation of an electromagnetic signal for any missileborne frequency to any instrumentation site. Clearly, such an exhaust plume ionization model would be most useful, and the accuracy to which attenuation could be predicted would depend on the accuracy of the model.

1. The Computation of Electromagnetic Wave Attenuation in an Inhomogeneous Medium

The computation of the attenuation of a signal through the plume requires the solution for the propagation of an electromagnetic wave through an inhomogeneous medium. While an analytic solution of this equation is not available (except for special, prescribed variations of electron density that do not correspond to the exhaust plume case), computer solutions are available. To obtain the attenuation through the plume, we have used an n-ply lossy multi-ply sandwich solution, available at AFETR as Computer Program DGWD No. 573, which treats the inhomogeneous plasma as a series (up to 250) of parallel layers of arbitrary thickness, arbitrary electron density, and arbitrary collision frequency.

2. Vicente Plume Model, Comparison with Flight Data

An exhaust plume ionization model, based on the gas-dynamic model of Vicente [17], was presented by Poehler [18] for the seven-segment, 120 inch Titan IIIC SRM. The model for the Titan IIIC vehicle is unclassified, and is shown in Figure 24.

It is of interest to test the Vicente model against flight test data, to see how well predicted attenuation compares with the X-, C-, S-, and P-band data collected on Test 8275/2250. Accordingly, attenuation computations were carried out for 10 and 15 degree rays through the plume. Rays from the antenna, at 10 and 15 degrees to the missile roll axis have been added to the Vicente model, which has been inclined to the missile roll axis to correspond to the 6 degree axis of the zero stage

Attenuation along 10 and 15 degree rays through the Vicente plume model were computed with the multi-ply computer program. The results are shown in Table III.

TABLE III
ATTENUATION CALCULATED FROM
VICENTE PLUME MODEL

Frequency MHz	Band	Attenuation, db 10^{o} Path	15^{o} Path
250	P	0.8	0
2200	S	0.01	0
5000	C	0.002	0
9100	X	0	0

Comparison of the computed predictions with the measured attenuation data given in Section IV, page 74, shows that predicted attenuation in orders of magnitude too low, further that the predicted attenuation does not extend to 15 degrees as the measured data shows.

FIG. 24 ZERO STAGE, TITAN IIIC, 120-INCH, 7-SEGMENT SRM PLUME AT 136,000 FEET (VICENTE MODEL)

(Model as published by Vicente, Reference 17, except for electron density N and collision frequency ν, which were computed from Vicente's data.)

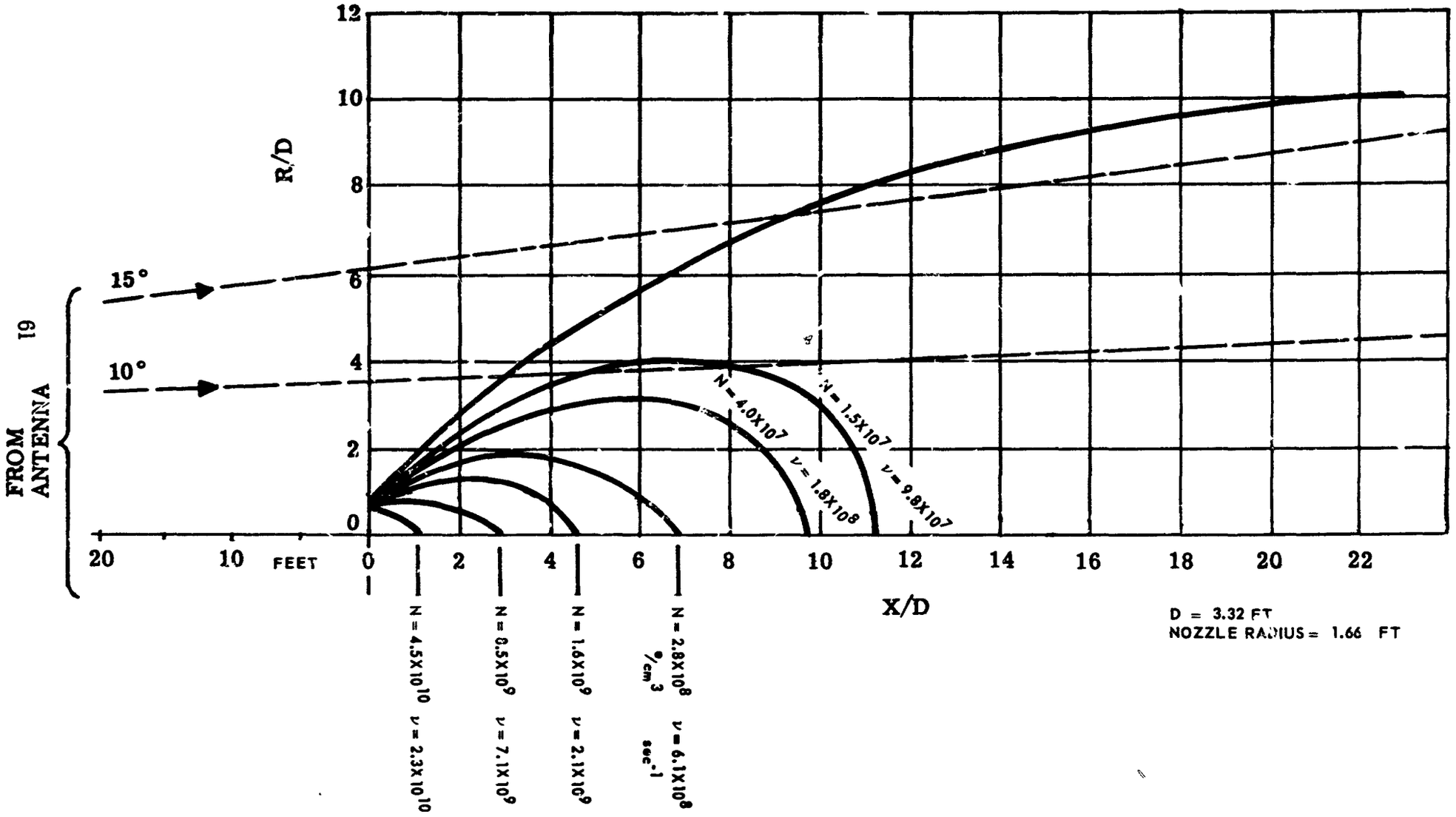

3. Empirical Plume Model, Comparison with Flight Data

It was felt useful to fashion a model that would more closely fit the experimental data. Clearly the electron density levels would have to be increased several orders of magnitude. Further, to account for the high attenuation at the edge of the plume, consideration was given to the afterburning ionization that was neglected in the Vicente model. As a model for the general shape of afterburning contours, the plume models published by Smoot [19] and by Jacobs [20], which included afterburning were used.

Essentially maintaining the basic flow field contours developed by Vicente, various levels of electron density and collision frequency/plasma frequency ratio were tried. For each model, attenuation along the 10 and 15 degree ray was computed by means of the multiply computer program, using as many as 23 slabs. In this manner, an empirical model of the Titan IIIC plume was arrived at that was in agreement with the measured attenuation data. This model is shown in Figure 25. The electron density variation along a 10 degree ray through this plume model is shown in Figure 26.

In Table IV we present a comparison of computed attenuation along the 10 and 15 degree rays through the empirical plume, with measured flight data.

b - $N = 9.4X10^8$ $\nu = 8X10^{10}$
c - $N = 4.6X10^9$ $\nu = 2.8X10^{11}$
d - $N = 2.6X10^{10}$ $\nu = 7.6X10^{11}$
e - $N = 5.7X10^{10}$ $\nu = 1.6X10^{12}$
f - $N = 4.2X10^8$ $\nu = 5.5X10^{10}$

FIG. 25 TITAN IIIC, 120 INCH, 5-SEGMENT, EXHAUST PLUME IONIZATION MODEL AT 130,000 FEET, (POEHLER MODEL).

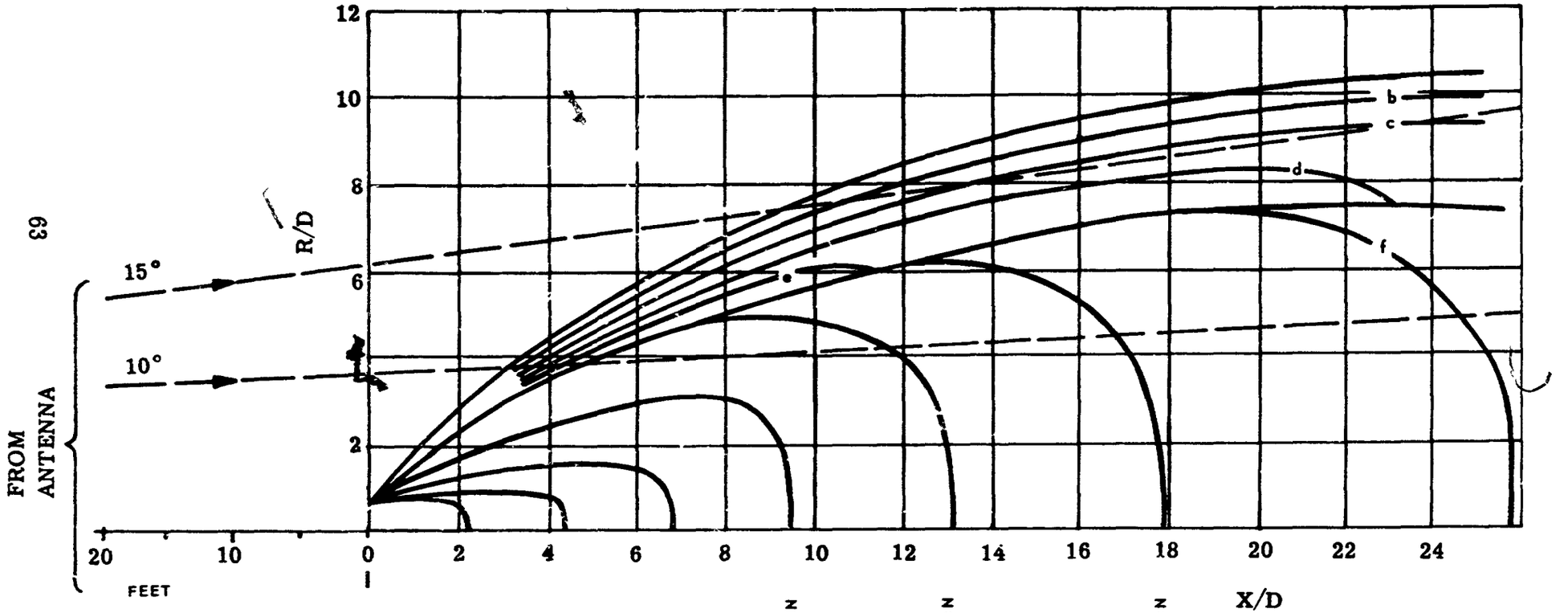

FIG. 26 ELECTRON DENSITY VARIATION ALONG A 10° DEGREE RAY THROUGH THE TITAN IIIC EXHAUST PLUME IONIZATION MODEL (POEHLER MODEL).

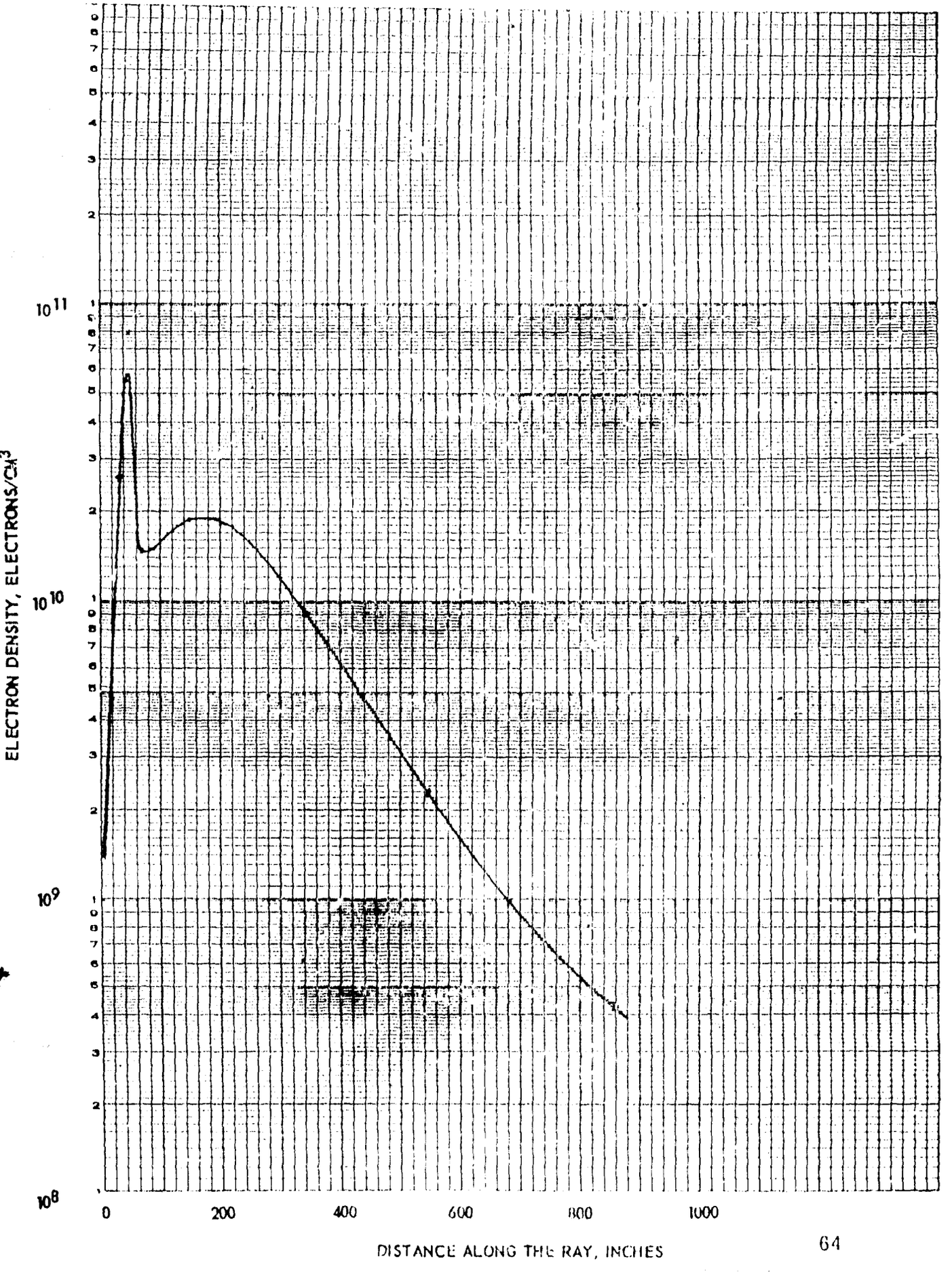

TABLE IV

ATTENUATION CALCULATED FROM THE EMPIRICAL PLUME MODEL (POEHLER MODEL), COMPARISON WITH FLIGHT DATA, TEST 8275

Frequency MHz	Band	Attenuation, db Calculated from Fig. 25	Flight Data
Along 10 Degree Ray			
250	P	14.6	< 15
2200	S	14.5	> 10
5000	C	14.1	> 10
9100	X	13.3	< 30
Along 15 Degree Ray			
250	P	14.9	< 15
2200	S	14.7	> 8
5000	C	14.1	—
9100	X	13.1	> 10

The agreement between the calculated and measured attenuation values is satisfactory. It is clear, however, that we are limited in our knowledge by the accuracy of the measurements obtained on Test 8275. In all too many cases, the sign "greater than" or "less than" appears.

Because of the construction of the Titan IIIC, the zero-stage exhaust plume is asymmetrical about the missile roll axis. We must, therefore, be careful to understand for which plane through the roll axis the empirical model of Figure 25 applies.

Since much of our data for the 10 and 15 degree path is in planes inclined approximately 45 degrees to the plane containing the roll and yaw axes (for angles of ϕ near 225 and 315 degrees), the empirical plume model should be interpreted as applying to a plane through the plume containing the roll axis and the line defined by ϕ = 225 degrees (or 315 degrees). Figure 27 clarifies orientation of these angles.

Since the plume is not symmetrical about the roll axis, our empirical model cannot be applied to the 5 degree data collected on Test 8275. Clearly another model in the ϕ = 180 plane is required. While the attenuation should not extend out to as wide an angle as 16 degrees, the electron intensity in this plane may well be higher because of the collision of the two zero-stage flow fields that would be expected in this plane.

4. Comparison, Vicente Model with Empirical Model

In order to arrive at a model that would agree with flight data it was necessary to (1) increase the electron density levels, (2) add afterburning contours, and (3) increase the collision frequency.

How reasonable are these modifications?

(1) The electron density levels presented by Vicente were too low because he computed his ionization levels on an assumed value of 100 ppm sodium, 0 ppm potassium impurity. Actually our measurements have shown, 360 ppm potassium and 380 ppm sodium to be in the zero-stage propellant. Since potassium is many times as effective as sodium in producing ionization, one should expect electron density levels many times higher than that used by Vicente.

(2) Afterburning in the exhaust was completely neglected in the Vicente model.

(3) An approximation of taking the collision frequency as that of "clean air" instead of computing the collision frequency for the molecular species actually present in the IIIC plume was employed by Vicente. While it is not obvious that the collision frequency will necessarily be higher, as our model indicates, clearly the collision frequency should be determined in a more rigorous manner.

FIG. 27 RAY THROUGH THE PLUME ILLUSTRATING ANTENNA ANGLES θ, ϕ, AND ASPECT ANGLE α

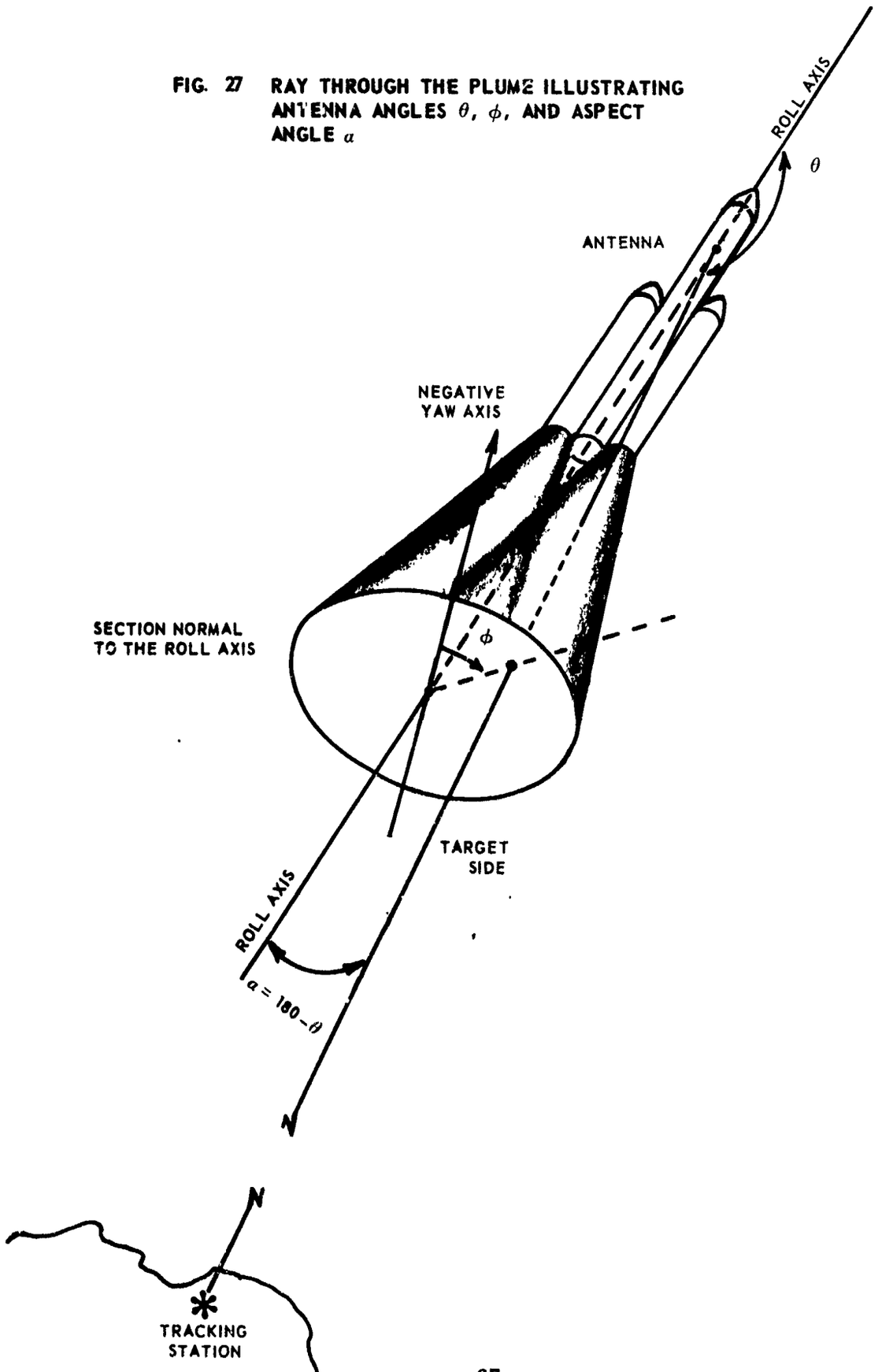

5. Improved Plume Models

As better flight data is collected, a more accurate empirical model can be developed. It is painfully obvious that our flight data on this test was all too often limited by "greater than" or "less than". The empirical model presented is consistent with the data available at this time. Better flight data is needed so that a more accurate empirical model can be fashioned.

An improved theoretical model is also needed: (1) The electron density at the exit plane should be derived using a considerably more accurate method, such as described by Smoot [19] and others, i.e., a treatment based on nonequilibrium processes of the ionic species uncoupled from those of the neutral species; the assumption of shifting equilibrium for the neutral species; and a derivation of the electron density at the exit plane by solution of the ionic material balances in the flow field environment. (2) The electron density calculations should be based on measured, not on assumed, values of alkali-metal impurities. (3) Afterburning phenomena should be considered. (4) The collision frequency should be determined by the standard method of determining the concentration of the various molecular species in the exhaust, and calculation of the collision frequency considering the temperature, concentration, and electron cross section of the various molecular species.

Through a marriage of an improved theoretical model with more accurate flight data, a highly accurate model can be developed that will serve a useful function in accurately predicting attenuation at any frequency and for any angle through the plume.

E. COMPLETED OSCILLOGRAMS

At the time the preliminary report was written, all the calibrations were not available. In particular, calibrations were omitted on the Oscillo Playback graphs at Site UC-2, UC-11, UC-13. The missing calibrations have been added. The completed graphs for UC-2, UC-11, and UC-13 are shown as Figures 28, 29, and 30. respectively.

Since flame attenuation is critically dependent on aspect angle, the values of aspect angles during the flight have been added for ready reference.

Since the companion [1] report was issued, S-band signal-strength levels at UC-11 and UC-13 have been re-calibrated, and small errors in the QLAP aspect-angle program have been corrected [21]. Both of these changes have been incorporated in Figures 28 - 30. The corrected aspect angles are listed in the Appendix for reference. The reader should update the aspect angles given in Figures 2 and 4 of the companion report [1] with the corrected angles.

FIG. 28 OSCILLO PLAYBACK, UC - 2, 0 - 150 sec, X, S

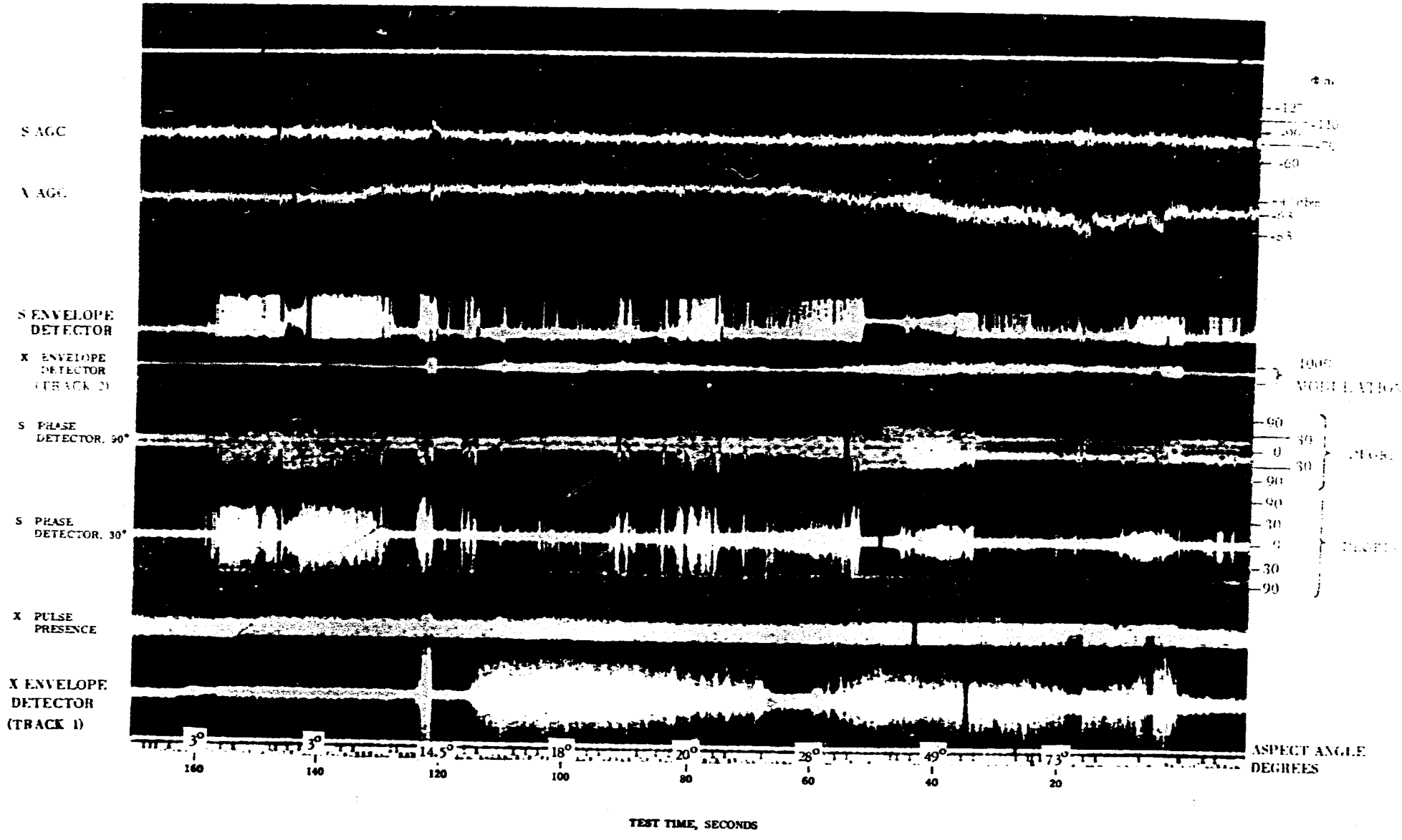

FIG. 29 OSCILLO PLAYBACK, UC-11, 0-150 sec, X, S

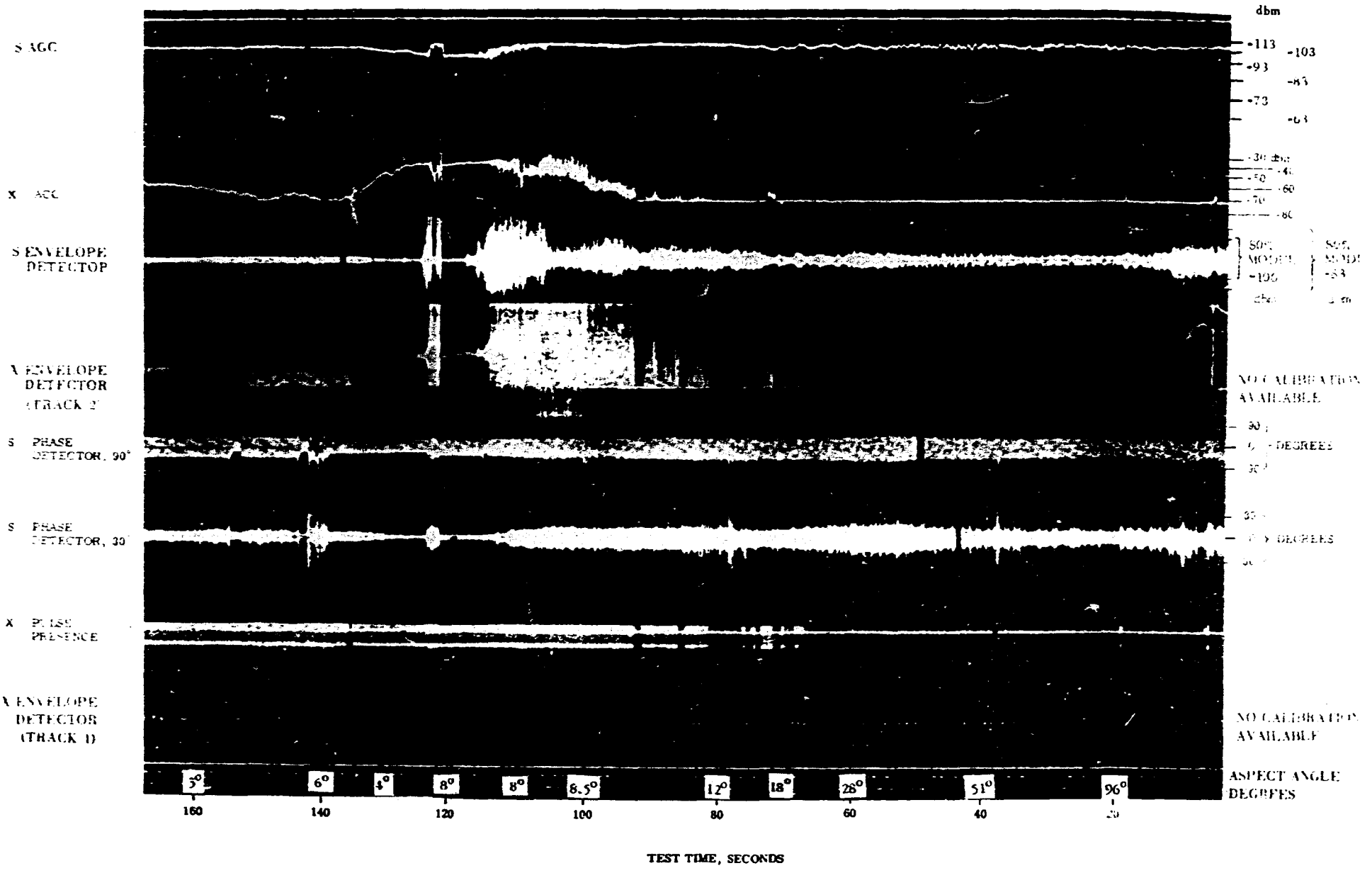

FIG. 30 OSCILLO PLAYBACK UC-13, 0 - 150 sec, X, S

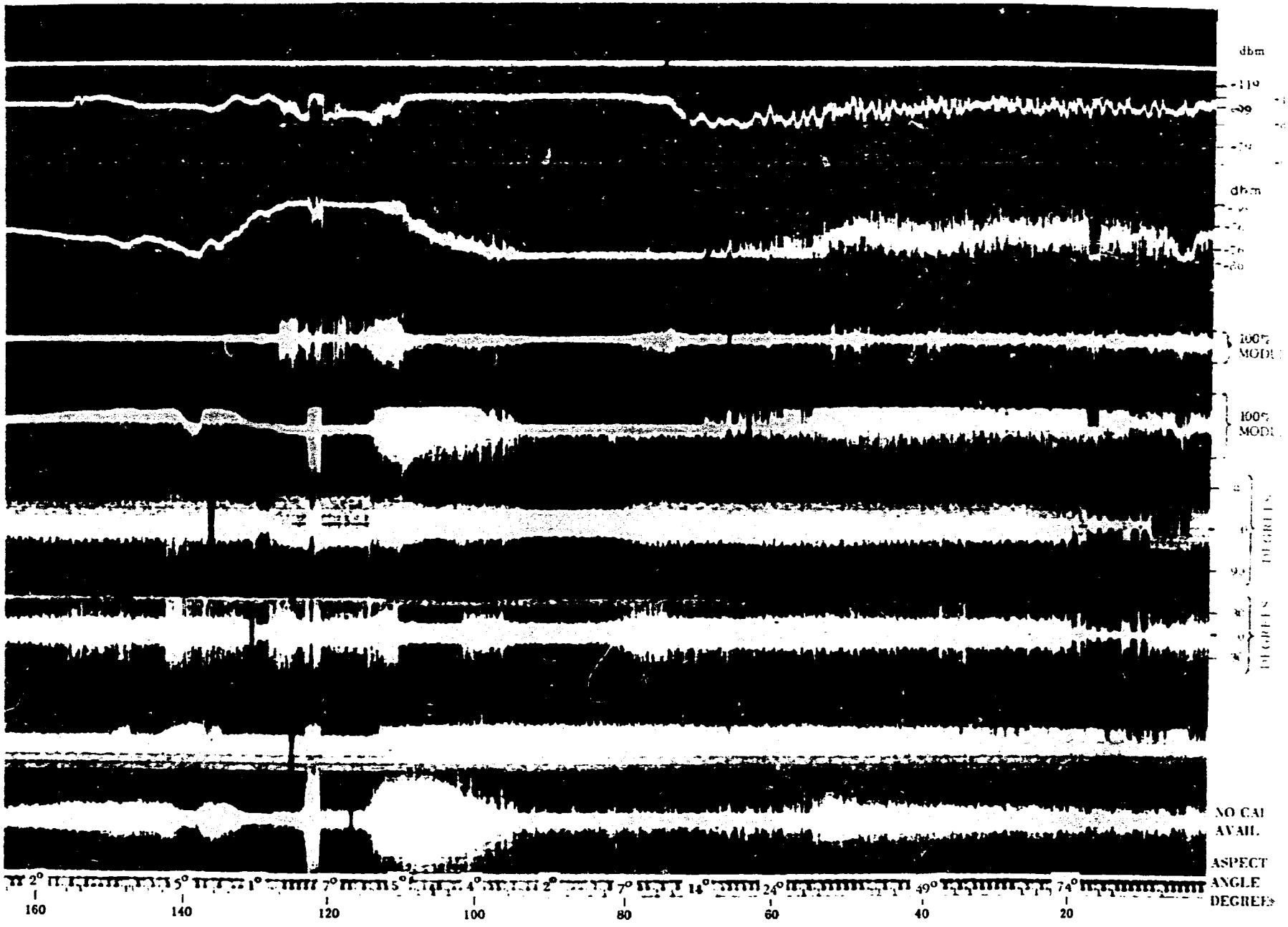

IV. SUMMARY OF ATTENUATION MEASUREMENTS

Details of the attenuation measurements have already been presented in the companion report [1], and, therefore, will not be repeated here. For reference, however, we will summarize the results of the attenuation measurements in Tables V, VI, VII and VIII. Note that Table V is labeled "signal loss" rather than attenuation, since the figures of this table may contain some cross-polarization losses, the magnitude of which could not be determined because the necessary antenna patterns were not provided with the antenna.

The corrections in S-band signal strength and in aspect angles, just discussed in Section III E, have been incorporated in Tables V - VIII.

TABLE V

X-Band Signal Loss**, Zero Stage

Aspect Angles*		Signal Loss	Test Time	Site
$\alpha = 180 - \theta$	ϕ			
> 16	70-150	0 db	0-110 sec	UC-2
16	339	> 10	+ 65	19.1
10-8	245-223	< 30	95-110	UC-11
9	186	30	108-110	19.1
4-5	199-188	40	100-110	UC-13

TABLE VI

C-Band Attenuation, Zero Stage

		Attenuation	Test Time	Site
> 15°	50-150	0 db	0-110 sec	CIF
11	346	> 10	+ 74	UC-13
6	188	> 20	+110	UC-13

TABLE VII

S-Band Attenuation, Zero Stage

> 25°	100-137	0 db	0-110 sec	STS
> 16	70-150	0	0-110	UC-2
> 15	50-150	0	0-110	CIF
15	306	> 8	+ 75	UC-11
10	346	> 12	+ 74	UC-13
8	223	> 10	+110	UC-11
5	188	> 20	+110	UC-13

TABLE VIII

P-Band Flame Attenuation, Zero Stage

> 15°	329-306	0 db	0- 75 sec	UC-11 (and UC-13)
8	223	15	+110	UC-11
5	191	15	+105	UC-13
2	281	20	+ 90	UC-13

P-Band Attenuation, Stage I

6°	188	20 db	+285	UC-13

* θ and ϕ are the standard antenna angles as defined in IRIG Document 111-65 "IRIG Standard Coordinate System and Data Format for Antenna Patterns," and are identical to Gamma 1 and Gamma 2 of [1], see Figure 27.

** Note the distinction between "signal loss" and "attenuation", spelled out in Section V.5 .

V. ITEMS FOR NEXT TIME

Certain deficiencies and omissions became apparent in the analysis of the data. These are pointed to so that they may be remedied on the next test.

1. Inadequate Time for Checkout

Many of the deficiencies and data problems can be traced back to a lack of time prior to the test. This problem must be recognized from the outset. Adequate time for checkout, debugging, and correct pre-flight calibration should be included in the test plan. Problems of high noise level, hum pickup, missing calibrations, distortion of calibrations manifested themselves in the data of this test, and unfortunately served to limit the usefulness of the data.

2. Checkout of Calibration Before Leaving the Site

An effective way to eliminate hum, distortion, and high noise levels in the calibrations is to assign responsibility to a particular engineer at each site, and require that he: (1) Play back all the pre-flight calibrations on oscilloscope prior to the test to check for a) limiting, b) saturation, c) noise level, d) overloading, and e) distortion; (2) Repeat the above procedure after the test, and be sure that no settings are changed until usable calibrations are furnished on tape.

3. Boresight Cameras

When signal is lost during the flame-attenuation period, the question of precisely where the antenna was pointing becomes crucial to the analysis. The proper solution to this problem is to install boresight cameras on all antennas, and to assure that correct alignment with the antenna is provided before the test. We made a request to have boresight cameras installed on all antennas for this test. Unfortunately, a shortage of time permitted only one camera to be mounted. Data from this camera was not usable since the camera was improperly aligned.

4. Correction of Frequency Instability of S-band Oscillator

The excessive frequency instability of the S-band transmitter made phase-locked track extremely difficult, and prevented us from obtaining phase noise data. When we are looking for flame-induced phase fluctuations, we should start with a stable oscillator, free from excessive frequency and phase fluctuations.

Steps should be taken to eliminate the frequency instability of the S-band oscillator. The oscillator should be sufficiently stable to operate with a phase-locked loop of less than 50 Hz loop bandwidth. Further, satisfactory operation with a phase-locked receiver should be exhibited when the transmitter package is exercised on a shake table with the maximum level, and with the frequency composition, of the vibration experienced on the missile during flight.

5. Missing X-Band Antenna Polarization Characteristics

The X-band antenna data supplied by the range user did not include the antenna polarization characteristics necessary to determine polarization losses. In our analysis of the flight data, we are, therefore, not able to define X-band flame attenuation, but restricted to reporting X-band "signal losses" which may contain some cross-polarization losses. The required antenna polarization characteristics are spelled out on pages 44-47 of the "IRIG Standard Coordinate System and Data Formats for Antenna Patterns," Document 111-65, published by the Secretariat, Range Commanders Council, White Sands Missile Range, New Mexico, 88002. The polarization characteristics may be spelled out either by the "Linear" or the "Circular Component Method" described in the reference document.

If it is not feasible to re-measure, and supply, the necessary antenna polarization characteristics, it is recommended that the receiving antennas be provided with circularly polarized feeds for the next test, so as to eliminate the cross polarization uncertainties.

VI. CONCLUSIONS AND RECOMMENDATIONS

The results of AFETR measurements on Titan IIIC, vehicle 10, Test 8275/2250 have shown:

1. The zero stage exhaust is severely attenuating at X, S, C, and P band. The attenuation extends to as far as 16 degrees, measured from the roll axis. "Signal losses" at X-band reached as high as 40 db, and flame attenuation reached values greater than 23 db at S-band, greater than 20 db at C-band, and values of 20 db at P-band. Note, however, lack of antenna polarization data does not permit us to separate cross-polarization losses at X-band. Therefore, the 40 db "signal loss" reported for X-band is an upper bound. Cross polarization losses must be subtracted from this figure to obtain X-band flame attenuation.

2. The zero-stage exhaust produces a severe degree of amplitude modulation of the signal passing through the plume. It is significant that the noise of the zero-stage is severe even when the attenuation is small. When the zero-stage thrust decays to less than 20%, the noise becomes negligible.

3. Amplitude flame noise is highest at low frequency, decreases with frequency, and reaches values as high as 10 db below the carrier per 50 Hz bandwidth at 100 cycles. Amplitude fluctuations of the carrier produced by the exhaust extend to 10 kHz for the separation-rocket exhaust.

4. The amplitude noise measurements reported herein are the only ones available for Titan IIIC. The noise that was measured was sufficiently severe and disturbing to range instrumentation that it is considered necessary to repeat these measurements on additional tests to obtain a measure of the repeatability of the measurements.

5. Flame-induced phase noise was observed, but no phase data was obtained on this test. To obtain this data on the next See-Thru test, it is essential that the frequency instability of the S-band oscillator be corrected. Because of the complete lack of flame-induced phase noise data on Titan IIIC, it is recommended that the phase-locked Glotrac system be utilized to collect phase noise data on the next three Titan IIIC tests.

6. The signal amplitude fluctuations produced by solid as well as liquid propellant flame noise have a probability distribution function that is very nearly Gaussian.

7. No pulse distortion by the rocket exhaust plume was observed. It is concluded that the Titan IIIC rocket exhaust plume is not a dispersive plasma. The exhaust plume serves to attenuate the pulse amplitude in a random manner, but does not affect the pulse shape otherwise.

8. An empirical exhaust plume ionization model that will explain the attenuation observed at X , C , S , and P band can be constructed from the flight data, and is presented in this report.

9. A very high alkali-metal impurity content (380 ppm Na, 360 ppm K) was measured on one sample of zero-stage propellant supplied by UTC. Additional measurements of the alkali-metal impurity should be made and correlated with attenuation.

10. The imposition of a specification for the maximum permissible level of sodium and potassium impurity in the zero-stage propellant is recommended to alleviate the rocket exhaust interference problems that the zero-stage rocket presents to the Air Force Western Test Range. A ten to one reduction in sodium and potassium impurity content of the propellant can be expected to give a three to one reduction in the number of decibels of attenuation at X , C , S , and P bands.

REFERENCES

[1] Poehler, H. A., "Project See-Thru, Flame Attenuation Interference Measurements, Titan IIIC Test 8275/2250, Preliminary Report," Technical Staff Memo No. 76, ETV-TM-68-6, 28 July 1967, Pan American World Airways, Patrick AFB, Fla., AD 624 034L.

[2] Ganschow, D. C., and Poehler, H.A., "Engineering Plan for Project See-Thru," Engineering Report No. 7300-50, 10 February 1967, Pan American World Airways, Patrick AFB, Fla.

[3] Memo, E. M. Fetner to H. A. Poehler, "Memo for the Record, Project See-Thru Debriefing for Test 8275/2250," 2 Oct. 1967, RCA Missile Test Project, Patrick AFB, Fla.

[4] Williams, H. , "Radio Scattering in Rocket Exhaust Jets," Presented at the December 7, 1967 Signal Transmission Working Group Meeting (STIP), Patrick AFB, Fla. To be published in the Proceedings Volume of this Working Group.

[5] Smoot, L. D. and Seliga, T. J., Jr., "Rocket Exhaust Plume Radar Attenuation and Amplitude/Phase Noise," Journal of Spacecraft and Rockets, Vol. 4, No. 6, June 1967, pp 774-780.

[6] Geiger, A. A., "Analysis of the Effects of Rocket Exhaust Fluctuations on FSK Telemetry," AIAA 6th Solid Propellant Rocket Conference, Preprint 65-184, Washington, D.C., 1-3 Feb. 1965.

[7] Poehler, H. A., "Observations of Radio Interference by Exhausts of Operating Missiles," Space Technology Laboratories Report No. GM-PTM-5656, 6 Sept. 1962, (Confidential). AD 336 179.

[8] Poehler, H. A., "Rocket Exhaust Plume Interference Problems - Current Status (U)," Report No. ETR-TR-67-8, June 1967, Pan American World Airways, Guided Missile Range Division, Patrick AFB, Fla. (Confidential). AD 384 414.

[9] Poehler, H. A., "Results of Special Flame Measurements of Titan IIIC Tests 3656/6025 and 6020/6546," Technical Staff Memo No. 54, ETV-TM-66-30, Pan American World Airways, Guided Missile Range Division, Patrick AFB, Fla., 15 June 1966. AD 824 033L.

[10] McPherron, T. R., and Fox, J. F., "Information Loss Caused by Reentry Plasma Dispersion," Proceedings of the Third Symposium of the Plasma Sheath-- Plasma Electromagnetics of Hypersonic Flight," Vol. III, pp 167-192, May 1967, Air Force Cambridge Research Laboratories, L. G. Hanscom Field Bedford, Mass.

[11] Hodara, H., Knop, C., and Marquedant, R., "Performance of Digital Signals Through Plasmas," IEEE Transactions on Communications Systems, March 1964, pp 74-86.

[12] Minutes of the Signal Transmission Working Group (STIP), Patrick AFB, Fla., 13 April 1967.

[13] Letter, T. L. War, Vice President Pacific Engineering and Production Co. of Nevada, Henderson, Nevada, to H. A. Poehler, 1 March 1968.

[14] Phelps, R. W., "Preliminary Flame Attenuation Predictions for Typical MOL Launches, (U)," Aerospace Corp., El Segundo, California, 1 Oct. 1965, Contract AF 04(695)-669, Report No. TOR-669(6107-25)-3. (Confidential).

[15] Letter, J. W. Jenney, American Potash and Chemical Corp., Los Angeles, Calif., to H. A. Poehler, Feb. 29, 1968.

[16] Telephone Conversation, March 31, 1968, T. L. War, Vice President Pacific Engineering and Production Co. of Nevada.

[17] Vicente, F. A., "Preliminary Flame Attenuation Analysis for Standard Launch Vehicles," Report No. TOR-669 (6107-25)-2, 1 Oct. 1965, Aerospace Corp., El Segundo, Calif. Contract No. AF 04(695)-669.

[18] Poehler, H. A., "A Survey of Exhaust Plume Models for Predicting Interference with Electromagnetic Wave Propagation," Technical Staff Memo No. 49, ETV-TM-66-24, ET66-15509, 29 April 1966, Pan American World Airways, Guided Missile Range Division, Patrick AFB, Fla. AD 375 207 (Secret).

[19] Smoot, L. D., and Underwood, D. L., "Prediction of Microwave Attenuation Characteristics of Rocket Exhausts," Journal of Spacecraft and Rockets, Vol. 3, No. 3, March 1966, pp 302-309.

[20] Jacobs, D. B., "Development of Saturn V Radio Flame Prediction Model - Final Report," The Boeing Co., Space Division Launch Systems Branch, 27 Feb. 1967, Report No. D5-15606-1.

[21] Erilane, R., "Radar Data from MVS Reconstruction SSLV C-10, Flight Plan 10-1," 8 June 1967, Aerospace Corporation, El Segundo California.

APPENDIX

A Listing of Corrected Antenna Angles* as Given by Erilane [21]

Test Time, SEC	UC-2		UC-11		UC-13	
	θ Degrees	Ø Degrees	θ Degrees	Ø Degrees	θ Degrees	Ø Degrees
50.8	143.8	94.3	142.2	329.8	144.8	353.8
55.3	148.1	98.5	147.5	327.6	150.3	353.2
61.3	152.7	105.3	153.9	323.4	157.1	351.9
65.8	155.2	111.0	158.3	319.1	161.8	350.7
70.3	157.3	116.9	162.0	313.4	166.0	348.5
74.8	158.6	122.5	165.4	306.5	169.8	346.5
80.8	160.2	130.0	168.5	293.4	174.0	338.1
85.3	161.0	135.6	170.0	280.6	176.4	320.4
91.0	161.6	140.4	171.5	263.0	178.2	262.8
95.8	161.9	147.3	170.7	245.3	176.1	217.8
100.3	162.4	147.1	171.6	236.1	175.8	199.6
106.2	163.4	148.6	172.0	226.1	175.0	189.8
110.8	164.5	149.6	172.2	222.4	174.8	188.1
115.3	165.0	152.2	171.8	217.2	173.9	187.7
121.3	165.7	155.3	171.4	212.5	173.1	187.6

* See Table V for definition of antenna angles.

Unclassified

Security Classification

DOCUMENT CONTROL DATA - R & D

(Security classification of title, body of abstract and indexing annotation must be entered when the overall report is classified)

1 ORIGINATING ACTIVITY *(Corporate author)* Pan American World Airways, ASD Patrick AFB, Fla. 32925	2a. REPORT SECURITY CLASSIFICATION Unclassified 2b GROUP N/A

3 REPORT TITLE

Project See-Thru Flame Interference Measurements, Titan IIIC Launch Test 8275/2250, Final Report

4 DESCRIPTIVE NOTES *(Type of report and inclusive dates)*

Final Report March 1968

5 AUTHOR(S) *(First name, middle initial, last name)*

Horst A. Poehler

6. REPORT DATE March 1968	7a. TOTAL NO. OF PAGES 89 incl Prefatory	7b NO OF REFS 21
8a. CONTRACT OR GRANT NO AF 08(606)-7500 b. PROJECT NO c. d.	9a. ORIGINATOR'S REPORT NUMBER(S) None 9b. OTHER REPORT NO(S) *(Any other numbers that may be assigned this report)* ETR-TR-68-3	

10 DISTRIBUTION STATEMENT Qualified requesters may obtain copies from Defense Documentation Center; each transmittal outside the agencies of the U. S. Government must have approval of New Systems Division, Directorate of Range Engineering, Air Force Eastern Test Range, Patrick AFB, Fla.

11 SUPPLEMENTARY NOTES	12 SPONSORING MILITARY ACTIVITY New Systems Division Directorate of Range Engineering, AFETR, AFSC, Patrick AFB, Fla.

13 ABSTRACT

A final report of flame attenuation, as well as flame noise measurements made at AF ETR on Titan IIIC, Test 8275/2250, April 28, 1967 is presented. Measurements were made at X-band(9100 MHz), C-band(5000MHz), S-band(2222 MHz), and P-band(220-250 MHz), frequencies at sites especially set up to yield a range of aspect angles, particularly at the low aspect angles of interest to AFWTR flights. Amplitude flame-noise measurements are reported for the first time for the Titan IIIC zero-stage. Power spectral density and probability distribution characteristics are presented. Also contained in this report are results of alkali-metal impurity measurements on the zero-stage, on the separation-rocket and the stage-I propellants; data on the effect of the exhaust flame on pulse transmission; and a plasma model of the zero-stage rocket exhaust from which predictions of rocket exhaust attenuation as a function of aspect angle and frequency can be made. The data indicates that at X-, S-, C-, and P-band frequencies, the zero-stage attenuation extends to approximately 16 degrees, measured from the roll axis. "Signal losses" at X band reached as high as 40 db, and flame attenuation reached values greater than db at S band, greater than 20 db at C band, and reached values of 20 db at P band. To alleviate the high zero-stage rocket exhaust attenuation, the imposition of a specification limiting the maximum permissible level of sodium and potassium impurity in the propellant is recommended.

DD FORM 1 NOV 65 1473

Unclassified

Security Classification

14 KEY WORDS	LINK A		LINK B		LINK C	
	ROLE	WT	ROLE	WT	ROLE	WT
Plasma Physics						
Propagation						
Ionization						
Attenuation						
Rocket Exhaust						
Plasma Medium						
Radar Attenuation						
Exhaust Flames						
Telemetry Systems Interference						
Radio Fr· quency Attenuation						
Flight Data Analysis						
Electromagnetic Wave Attenuation						

AFSC - Patrick AFB, Fla.